

# METAL: The Metal Evolution, Transport, and Abundance in the Large Magellanic Cloud Hubble program. IV. Calibration of Dust Depletions vs Abundance Ratios in the Milky Way and Magellanic Clouds and Application to Damped Lyman- $\alpha$ Systems

JULIA ROMAN-DUVAL,<sup>1</sup> EDWARD B. JENKINS,<sup>2</sup> KIRILL TCHERNYSHYOV,<sup>3</sup> CHRISTOPHER J.R. CLARK,<sup>1</sup> ANNALISA DE CIA,<sup>4</sup>  
KARL GORDON,<sup>1</sup> ALEKSANDRA HAMANOWICZ,<sup>1</sup> VIANNEY LEBOUTELLER,<sup>5</sup> MARC RAFELSKI,<sup>1</sup> KARIN SANDSTROM,<sup>6</sup>  
JESSICA WERK,<sup>3</sup> AND PETIA YANCHULOVA MERICA-JONES<sup>1</sup>

<sup>1</sup>*Space Telescope Science Institute  
3700 San Martin Drive  
Baltimore, MD21218, USA*

<sup>2</sup>*Department of Astrophysical Sciences  
Peyton Hall, Princeton University  
Princeton, NJ 08544-1001 USA*

<sup>3</sup>*Department of Astronomy  
Box 351580, University of Washington  
Seattle, WA 98195, USA*

<sup>4</sup>*Department of Astronomy, University of Geneva  
Chemin Pegasi 51  
1290 Versoix, Switzerland*

<sup>5</sup>*AIM, CEA, CNRS, Université Paris-Saclay, Université Paris Diderot, Sorbonne Paris Cité  
F-91191 Gif-sur-Yvette, France*

<sup>6</sup>*Center for Astrophysics and Space Sciences, Department of Physics  
University of California  
9500 Gilman Drive  
La Jolla, San Diego, CA 92093, USA*

(Accepted June 9, 2022)

Submitted to ApJ

## ABSTRACT

The evolution of the metal content of the universe can be tracked through rest-frame UV spectroscopy of damped Ly- $\alpha$  systems (DLAs). Gas-phase abundances in DLAs must be corrected for dust depletion effects, which can be accomplished by calibrating the relation between abundance ratios such as [Zn/Fe] and depletions (the fraction of metals in gas, as opposed to dust). Using samples of gas-phase abundances and depletions in the Milky Way (MW), LMC, and SMC, we demonstrate that the relation between [Zn/Fe] and other abundance ratios does not change significantly between these local galaxies and DLAs, indicating that [Zn/Fe] should trace depletions of heavy elements in those systems. The availability of photospheric abundances in young massive stars, a proxy for the total (gas+dust) metallicity of neutral gas, in the MW LMC, and SMC allows us to calibrate the relation between [Zn/Fe] and depletions in these nearby galaxies. We apply the local calibrations of depletions to DLA systems. We find that the fraction of metals in dust, the dust-to-gas-ratio, and total abundances are 2-5 times lower than inferred from previous depletion calibrations based on MW measurements and a different formalism. However, the trend of dust abundance vs. metallicity remains only slightly sub-linear for all existing depletion calibrations, contrary to what is inferred from FIR, 21 cm, and CO emission in nearby galaxies and predicted by chemical evolution models. Observational constraints on the FIR dust opacity and depletions at metallicities lower than 20% solar will be needed to resolve this tension.

*Keywords:* Interstellar medium (847), Interstellar dust processes (838), Galaxy chemical evolution (580), Gas-to-dust ratio (638), Interstellar abundances (832), Damped Lyman-alpha systems (349)

## 1. INTRODUCTION

Metals (i.e., elements heavier than helium) are formed within stars and disseminated into the interstellar medium (ISM) by the powerful winds of massive stars and by supernova explosions, where they are re-incorporated into future generations of stars. A substantial fraction of those metals is ejected into the halos of galaxies, where they can remain or "rain" back into the ISM. More than 90% of the baryons reside in the gaseous phase of the universe (Péroux & Howk 2020), and a substantial fraction of metals in the universe are found in neutral gas. An inventory of metals in neutral gas over cosmic times is therefore necessary to understand the formation and evolution of galaxies and stars within them.

An efficient and accurate approach to measure the evolution of the neutral gas metal content of the universe is through the rest-frame UV spectroscopy of damped Ly- $\alpha$  systems (DLAs). DLAs are neutral gas absorption systems with  $\log N(\text{H I}) > 20.3 \text{ cm}^{-2}$  observed over a wide range of redshifts using quasar absorption spectroscopy (e.g., Rafelski et al. 2012; Quiret et al. 2016; De Cia et al. 2018). DLAs dominate the neutral gas content of the universe out to  $z \sim 5$  (Prochaska et al. 2005; O'Meara et al. 2007) and carry the majority of metals at high redshift (Péroux & Howk 2020). Because DLAs are detected via the absorption lines they produce, their abundance measurements are insensitive to excitation conditions, and unbiased with respect to mass and luminosity, making them an ideal tracer of the chemical enrichment of the universe.

However, gas-phase abundance measurements in DLAs have to be corrected for the depletion of metals from the gas to the dust phase, particularly at metallicities  $>1\%$  solar, where a significant fraction of metals resides in the dust phase. Such corrections have been derived from gas-phase abundance ratios of volatile elements (e.g., Zn, S) to refractory elements (e.g., Fe, Si), owing to the different rates at which these two types of elements deplete (De Cia et al. 2013). Zn being the least depleted volatile, and Fe being one of the most depleted and easiest to measure refractory elements, the gas-phase  $[\text{Zn}/\text{Fe}]$  abundance ratio is commonly used as a tracer of dust depletion in DLAs (Noterdaeme et al. 2008; De Cia et al. 2013, 2016).

The corrections for depletion effects in DLA gas-phase abundances also probe the evolution of the cosmic den-

sity of dust (Péroux & Howk 2020), and the relation between metal content (metallicity) and dust abundance, i.e., the dust-to-gas ratio or D/G (Galliano et al. 2018; Péroux & Howk 2020). Such studies have revealed a tension between the metallicity-D/G relation obtained in DLAs using  $[\text{Zn}/\text{Fe}]$  to trace the dust content of neutral gas, and that obtained in nearby galaxies by using FIR to trace their dust content, HI 21 cm to trace their neutral gas, and CO (1-0) emission to trace their molecular gas (see Figure 9a in Galliano et al. 2018). In nearby galaxies observed in emission (FIR, 21 cm, CO), the D/G drops abruptly below a critical metallicity of about 10% solar, an effect explained in chemical evolution models by the insufficient rate of dust growth in the ISM to counteract dust destruction by interstellar shocks and dust dilution by pristine inflows (Feldmann 2015). Conversely in DLAs, the D/G decreases only slightly faster than (sub-linearly with) metallicity. At low metallicities ( $< 10\%$  solar), this results in a discrepancy between the two types of samples and measurements amounting to a factor of a few to an order of magnitude in the dust abundance for a given metallicity.

This tension could be explained by a number of systematic effects in either or both approaches. The systematic effects affecting D/G measurements from FIR, 21 cm and CO emission are described in Roman-Duval et al. (2014, 2021). They include systematic uncertainties on the FIR opacity of dust (factor of a few), the CO-to-H<sub>2</sub> conversion factor (Bolatto et al. 2013), and coverage differences between HI 21 cm and dust emission. D/G estimates in DLAs are not devoid of potential systematics either. For example, the relation between the gas-phase  $[\text{Zn}/\text{Fe}]$  ratio and dust depletion corrections in DLAs relies in part on a calibration of the relation between  $[\text{Zn}/\text{Fe}]$  and the depletion of Zn obtained in the MW at solar metallicity (De Cia et al. 2016). It is possible that nucleosynthetic effects for Zn modify this relation at low metallicity. Indeed, Zn could behave like an  $\alpha$ -process element (Ernandes et al. 2018), with the stellar  $[\text{Zn}/\text{Fe}]$  ratio being enhanced in some stellar populations in an age and metallicity-dependent way (Duffau et al. 2017; da Silveira et al. 2018; Delgado Mena et al. 2019). Similarly, nucleosynthetic effects for  $\alpha$ -elements were accounted for in the depletion corrections developed for DLAs, but rely on abundance measurements in MW stars and un-depleted low-metallicity

DLAs.

Fortunately, large samples of interstellar abundance and depletions have recently become available outside the Milky Way, specifically in the Large and Small Magellanic Clouds (Tchernyshyov et al. 2015; Jenkins & Wallerstein 2017; Roman-Duval et al. 2021). The LMC and SMC have metallicities 50% and 20% solar respectively (Russell & Dopita 1992), and so those abundance and depletion samples can be used to test whether the dust corrections used in DLAs hold at metallicities lower than solar. Based on those samples, Roman-Duval et al. (2022, hereafter Paper III) establish that the relation between the depletions of different elements does not vary significantly between the MW, LMC and SMC. Subsequently, the relation between different abundance ratios remains relatively invariant with metallicity, at least above the metallicity of the SMC. This is consistent with the findings presented in De Cia (2018), who also compared the relation between abundance ratios in the MW, LMC and SMC, albeit with the significantly smaller LMC sample available at the time.

In this paper, we use recent abundance and depletion samples obtained in the MW, LMC and SMC to calibrate the relation between  $[\text{Zn}/\text{Fe}]$  and depletions. We thereby derive new dust depletion corrections that can readily be applied to gas-phase abundance measurements in DLAs in order to estimate their metal and dust content. Furthermore, we estimate the dust abundance in DLAs based on these dust corrections and examine the relation between metallicity and D/G obtained in each case (MW, LMC, or SMC calibration). We compare the new dust corrections, the metallicity-D/G relation, and the redshift evolution of DLA metallicities obtained in this work with those derived from previous work in the literature.

The paper is organized as follows. In Section 2, we provide some background and summarize the samples and approach used to determine depletions, D/G, and D/M in the MW, LMC, SMC, and DLAs. In Section 3, we compare the D/G obtained from the De Cia et al. (2016) calibration of depletions vs  $[\text{Zn}/\text{Fe}]$  with the D/G measurements obtained in nearby galaxies from FIR, 21 cm, and CO emission. The resulting tension between the two types of D/G measurements motivates the need to investigate alternate depletion calibrations. Calibrations of depletions as a function of  $[\text{Zn}/\text{Fe}]$  derived in the MW, LMC, and SMC are presented in Section 4. In Section 5, we apply the new depletion calibrations established in the MW, LMC, and SMC to estimate depletions, D/G, and the dust composition in DLAs. We also examine the redshift evolution of DLA metallicities and the trend of D/G vs metallicity with these new

calibrations. We provide a summary of the results in Section 6.

## 2. INTERSTELLAR DEPLETIONS, D/M, AND D/G IN THE MW, LMC, SMC AND DLAS

The depletion of element X,  $\delta(X)$ , is the logarithm of the fraction of X in the gas-phase, and is given by:

$$\delta(X) = \log_{10} \left( \frac{N(X)}{N(\text{H})} \right) - \log_{10} \left( \frac{N(X)}{N(\text{H})}_{\text{tot}} \right) \quad (1)$$

$N(X)$  is the column density of element X along the line-of-sight, and  $(X/H)_{\text{tot}}$  are total (gas + dust) ISM abundances. In nearby galaxies where stellar abundances can be measured, total interstellar abundances are assumed to equate the photospheric abundances of young stars recently formed out of the ISM. In the following sections, we detail how depletions are derived in nearby galaxies and DLAs, and specify the samples used in this analysis.

### 2.1. Derivation and samples of depletions in the MW, LMC, and SMC

In the MW, LMC, and SMC, where stellar abundances can be measured, total ISM abundances,  $(X/H)_{\text{tot}}$ , are assumed to equate the abundances in the photospheres of young stars recently formed out of the ISM. For these galaxies, we use the samples of abundance and depletions compiled in Paper III, which are based on studies by Jenkins (2009) (MW, 226 sight-lines), Roman-Duval et al. (2021) (LMC, 32 sight-lines), and Jenkins & Wallerstein (2017) (SMC, 18 sight-lines). The column density measurements compiled from these studies are modified by Paper III to assume the same set of oscillator strengths. The depletion samples from Paper III rely on the stellar abundances listed in their Table 1. For convenience, stellar abundances assumed in the MW, LMC, and SMC are repeated here in Table 1.

In this paper, we make use of the formalism introduced by Jenkins (2009) based on the  $F_*$  parameter relating the depletions of different elements, which are observed to correlate tightly together.  $F_*$  therefore describes the collective advancement of depletions.  $F_*$  was defined in the MW, with  $F_* = 0$  corresponding to the least depleted sight-lines in the MW with  $\log N(\text{H}) > 19.5 \text{ cm}^{-2}$  (implying negligible ionization corrections) and  $F_* = 1$  corresponding to the most depleted velocity component toward  $\zeta$  Oph. Following Jenkins (2009), the depletion of element X can be modeled from  $F_*$  by:

$$\delta(X) = A_X(F_* - z_X) + B_X \quad (2)$$

**Table 1.** Reference stellar abundances (a proxy for the ISM total abundances) in the MW, LMC, SMC

Element	$W_X^a$	MW $12+\log(X/H)_{\text{tot}}$	Ref <sup>b</sup>	LMC $12+\log(X/H)_{\text{tot}}$	Ref <sup>b</sup>	SMC $12+\log(X/H)_{\text{tot}}$	Ref <sup>b</sup>
C	12.01	8.46	1	7.94	2	7.52	2
O	16.0	8.76	1	8.50	2	8.14	2
Mg	24.3	7.62	1	7.26	2	6.95	6
Si	28.1	7.61	1	7.35	2	6.86	6
S	32.06	7.26	1	7.13	3	6.47	6
Ti	47.87	5.00	1	4.76	4	4.30	6
Cr	52.0	5.72	1	5.37	2	4.99	6
Fe	55.85	7.54	1	7.32	2	6.85	6
Ni	58.7	6.29	1	5.92	2	5.57	6
Cu	63.55	4.34	1	3.79	5	...	...
Zn	65.4	4.70	1	4.31	2	3.91	6

<sup>a</sup>Atomic weight

<sup>b</sup>(1) Jenkins (2009), who adopt proto-solar abundances from Lodders (2003); (2) Tchernyshyov et al. (2015); (3)  $12 + \log(S/H) = [S/Fe] + (S/Fe)_\odot + 12 + \log(Fe/H)$  with  $[S/Fe]$  from Hill et al. (1995),  $12 + \log(Fe/H)$  from (2), and  $(S/Fe)_\odot$  from Lodders (2021); (4) Welty & Crowther (2010); (5) Asplund et al. (2009) scaled by factor 0.5 (−0.3 dex); (6) Jenkins & Wallerstein (2017), who scale proto-solar abundances from Lodders (2003) by a factor 0.22 (−0.6 dex)

where the  $A_X$ ,  $B_X$  and  $z_X$  coefficients are obtained from examining and fitting the relation between depletion measurements for different elements toward a sufficiently large sample of sight-lines. The term  $z_X$  is introduced to remove the covariance between errors on the slope ( $A_X$ ) and intercept ( $B_X$ ) of the relation. The  $F_*$  parameter is critical in inferring depletions for elements when they cannot be measured.

Table 2 of Paper III lists the  $A_X$ ,  $B_X$  and  $z_X$  coefficients determined in the MW, LMC, and SMC, accounting for the adjustments of oscillator strengths to make the three local samples consistent. For convenience, we repeat these coefficients here in Table 2. The  $B_X$  coefficients rely on assumed stellar abundances listed in Table 1.

## 2.2. Deriving depletions in DLAs

In DLAs, depletions cannot be measured in the same way as in local galaxies, because stellar abundances are not known in those systems. However, depletions in DLAs can be inferred from the gas-phase  $[Zn/Fe]$  abundance ratio, or similarly a gas-phase abundance ratio of a volatile element to a refractory element. Specifically, the abundance ratio of element X to element Y relative

to solar,  $[X/Y]$ , is related to the depletions of X and Y,  $\delta(X)$  and  $\delta(Y)$  by:

$$\left[\frac{X}{Y}\right] = \delta(X) - \delta(Y) + \alpha(X) - \alpha(Y) \quad (3)$$

where  $\alpha(X)$  is the over- or under-abundance of X with respect to Fe relative to the solar  $(X/Fe)_\odot$  ratio ( $\alpha(X) = [X/Fe]$ , where  $[X/Fe]$  is measured in stars).  $\alpha(X)$  accounts for nucleosynthetic effects, in particular in  $\alpha$ -elements (e.g., Si, S, Mg). We emphasize that  $\alpha(X)$  refers to abundance variations relative to solar excluding the effects of depletions, and can be measured either in stars (in nearby galaxies) or un-depleted DLAs (De Cia et al. 2016).

De Cia et al. (2016, hereafter DC16) constrain the relation between depletions of various elements and the gas-phase  $[Zn/Fe]$  abundance ratio in DLAs, resulting in the following relation:

$$\delta(X) = A_2(X) + B_2(X) \times [Zn/Fe] \quad (4)$$

where the coefficients  $A_2$  and  $B_2$  are given in their Table 3. In a nutshell, the methodology used by DC16 to derive the  $A_2$  and  $B_2$  coefficients in those systems is the following:

1. First,  $\delta(X)$  is expressed as a function of the abundance ratio  $[X/Zn]$ , the depletion of Zn, and the

**Table 2.**  $A_X$ ,  $B_X$ , and  $z_X$  coefficients relating depletions and  $F_*$  in the MW, LMC, and SMC

Element	$A_X$			$B_X$			$z_X$		
	MW	LMC	SMC	MW	LMC	SMC	MW	LMC	SMC
C	-0.10±0.23	...	...	-0.19±0.06	...	...	0.803	...	...
O	-0.23±0.05	...	...	-0.14±0.05	...	...	0.598	...	...
Mg	-1.00±0.04	-0.60±0.11	-0.25±0.26	-0.80±0.02	-0.50±0.02	-0.33±0.03	0.531	0.407	0.162
Si	-1.14±0.06	-1.11±0.12	-1.05±0.09	-0.57±0.03	-0.68±0.03	-0.36±0.02	0.305	0.247	0.129
S	-0.879±0.28	-1.02±0.10	-0.87±0.14	-0.091±0.04	-0.31±0.02	-0.02±0.04	0.290	0.137	0.106
Ti	-2.05±0.06	-1.48±0.15	-1.45±0.09	-1.96±0.03	-1.63±0.02	-1.23±0.02	0.430	0.401	0.189
Cr	-1.45±0.06	-1.18±0.08	-1.33±0.16	-1.51±0.06	-1.13±0.02	-0.93±0.02	0.470	0.368	0.155
Fe	-1.28±0.04	-1.28±0.04	-1.28±0.07	-1.51±0.03	-1.51±0.03	-1.18±0.02	0.437	0.437	0.181
Ni	-1.49±0.06	-1.29±0.08	-1.41±0.14	-1.83±0.04	-1.26±0.02	-1.11±0.02	0.599	0.338	0.141
Cu	-0.71±0.09	-1.15±0.42	...	-1.10±0.06	-0.44±0.09	...	0.711	0.325	...
Zn	-0.61±0.07	-0.73±0.07	-0.51±0.14	-0.38±0.04	-0.36±0.02	-0.31±0.02	0.555	0.358	0.168

$\alpha$ -enhancement of X and Zn using Equation 3, i.e. via  $\delta(X) = [X/Zn] + \delta(Zn) - \alpha(X) + \alpha(Zn)$  (Equation 3 of DC16). DC16 assume that Zn has a nucleosynthetic history similar to Fe, and therefore  $\alpha(Zn)=0$ , but note that Zn is strictly not an iron-peak element, and that there could be small  $[Zn/Fe]$  nucleosynthetic variations. The enhancement of X relative to Fe,  $\alpha(X)$ , is measured in stars and un-depleted DLAs (their Figure 7).

2. Second, a linear function between  $[X/Zn]$  and  $[Zn/Fe]$ , with coefficients  $A_1$  and  $B_1$  is determined from fits to abundance ratios observed in DLAs (their Figure 3). The  $A_1$  and  $B_1$  coefficients are listed in Table 2 of DC16.
3. The third step consists in calibrating the linear relation with zero-intercept between  $\delta(Zn)$  and  $[Zn/Fe]$  using  $\delta(Zn)$  and  $[Zn/Fe]$  measurements in the MW, where depletions can be measured from ISM and stellar abundances (Figure 5 of DC16). This explicitly assumes  $\delta(Zn) = 0$  at  $[Zn/Fe] = 0$ .
4. Lastly, combining steps 1-3,  $\delta(X)$  can be expressed as a linear function of  $[Zn/Fe]$  (Equation 5 of DC16), with coefficients  $A_2$  and  $B_2$  listed in their Table 3.

A key goal of the work presented in the following is to use the depletions observed in the MW, LMC, and SMC to provide additional constraints on the relation between  $[Zn/Fe]$  and depletions, and examine how this relation may vary between systems and with metallicity (see Section 5.2). As stated in the Introduction, there exists a tension between the metallicity-D/G relation estimated

in DLAs from  $[Zn/Fe]$  and observed in nearby galaxies from FIR + 21 cm + CO (1-0) emission. This paper aims to determine whether systematic variations in the relation between  $[Zn/Fe]$  and depletions with metallicity can resolve this tension.

### 2.3. Samples of DLA abundances and depletions

In this work, we make use of the DLA gas-phase abundances for O, Mg, Si, S, Fe, Cr, Zn compiled by DC16 (their Table F2) and [Quiret et al. \(2016\)](#). Since a measurement of  $[Zn/Fe]$  is required to estimate the depletions of different elements in those systems, we only retain the DLAs for which Fe and Zn abundance measurements (not limits) are available. There are 34 such systems (out of 70) published in DC16 and 116 DLAs and sub-DLAs with both Zn and Fe measurements in [Quiret et al. \(2016\)](#) (out of 319 published).

Since we compare abundance ratios and depletions between the MW, LMC, SMC, and DLA systems, we need to ensure that all samples assume the same oscillator strengths. DC16 assume the oscillator strength from [Kisielius et al. \(2014\)](#) for S II, while the f-value from [Morton \(2003\)](#) are assumed for the MW, LMC, and SMC. To homogenize the column density determinations, we lower the column densities of S from DC16 by 0.04 dex, making those estimates consistent with the [Morton \(2003\)](#) oscillator strengths for S II. Lastly, we note that the abundances relative to solar listed in DC16 assume different solar abundances from [Jenkins \(2009\)](#): DC16 take their solar abundances from [Asplund et al. \(2009\)](#) while [Jenkins \(2009\)](#) assumes proto-solar abundances from [Lodders \(2003\)](#). However, the solar abundances assumed in these two studies are offset by the same amount for Zn and Fe, such that  $[Zn/Fe]$  remains

invariant under either assumption. Therefore, the  $A_2$  and  $B_2$  coefficients are not impacted by the assumption on solar abundances. Nevertheless, we scale the DC16 abundances relative to solar to assume the [Lodders \(2003\)](#) values as in [Jenkins \(2009\)](#).

The sample of DLA abundances compiled by [Quiret et al. \(2016\)](#), which includes many datasets and studies referenced in their Table B1, assumes oscillator strengths for Zn II from [Morton \(2003\)](#), while the MW, LMC, SMC and DC16 studies take their Zn II values from [Kisielius et al. \(2015\)](#). To make our sample self-consistent, we therefore lower the column densities of Zn listed in [Quiret et al. \(2016\)](#) by 0.1 dex, equivalent to using the [Kisielius et al. \(2015\)](#) oscillator strength for Zn II.

The compilation of DLA abundances by [Quiret et al. \(2016\)](#) includes both DLA ( $\log N(\text{H I}) > 20.3 \text{ cm}^{-2}$ ) and sub-DLA systems with  $\log N(\text{H I}) < 20.3 \text{ cm}^{-2}$ . Sub-DLAs are more susceptible to ionization effects (meaning that the first ion for which abundances are measured may not be the dominant ion). While several studies ([jen 2004](#); [Jenkins 2009](#); [Tchernyshyov et al. 2015](#)) have shown that such ionization corrections are negligible for  $\log N(\text{H}) > 19.5 \text{ cm}^{-2}$  in nearby galaxies, this is not true at high redshift. For example, [Fumagalli et al. \(2016, their Figure 2\)](#) have shown that the fraction of doubly ionized carbon in Lyman-limit systems is significant at redshift  $> 0$ , even for  $\log N(\text{H}) > 19 \text{ cm}^{-2}$ . Therefore, we do not include sub-DLA systems in this work, which removes 18 sub-DLA systems from the [Quiret et al. \(2016\)](#) sample, bringing the total number of systems to 98.

For both samples of DLAs ([De Cia et al. \(2016\)](#) and [Quiret et al. \(2016\)](#)), we then apply Equation 4 to the observed gas-phase  $[\text{Zn}/\text{Fe}]$  abundance ratio to estimate depletions for the DLA compilations. We caution that the selection of our sample based on the detection of Zn implies a bias toward higher metallicity systems ( $> 1\%$  solar). For lower metallicity systems where Zn cannot be detected, other depletion indicators, such as  $[\text{Si}/\text{Fe}]$  would be required. However, establishing the calibration of depletions vs  $[\text{Si}/\text{Fe}]$  is a difficult task outside the scope of this paper, because Si is  $\alpha$ -enhanced in way that depends on the star-formation history of the system. We therefore leave the calibration of abundance ratios detectable in the lowest metallicity DLAs to a future paper.

#### 2.4. Derivation of $D/G$ and $D/M$

$D/G$  and  $D/M$  can be computed from abundances, which provides the mass of metals available to form and dust, and depletions, which constrain the fraction of those metals in dust.  $D/G$  and  $D/M$  are given by:

$$D/G = \frac{1}{1.36} \sum_X (1 - 10^{\delta(X)}) \left( \frac{N(X)}{N_{\text{H}}} \right)_{\text{tot}} W_X \quad (5)$$

and,

$$D/M = \frac{\sum_X (1 - 10^{\delta(X)}) \left( \frac{N(X)}{N_{\text{H}}} \right)_{\text{tot}} W_X}{\sum_X \left( \frac{N(X)}{N_{\text{H}}} \right)_{\text{tot}} W_X} \quad (6)$$

where  $(N(X)/N_{\text{H}})_{\text{tot}}$  is the total abundance of element X in a galaxy or DLA and  $W_X$  is the atomic weight of element X.

For the MW, LMC and SMC,  $(N(X)/N_{\text{H}})_{\text{tot}}$  are the stellar abundances taken from Table 1 (see Section 2.1). The  $D/G$  and  $D/M$  in the MW, LMC and SMC were derived in Paper III (their Figures 5, 6, 7, and Table 5).

In DLAs, we estimate total abundances from the depletions, gas-phase abundances, and Equation 1, i.e.,  $(N(X)/N_{\text{H}})_{\text{tot}} = (N(X)/N_{\text{H}})_{\text{gas}}/10^{\delta(X)}$ . In this case, the depletions are inferred from the  $[\text{Zn}/\text{Fe}]$  abundance ratio as described in Section 2.2 (while they are inferred from the logarithm of the ratio of gas-phase to stellar abundances in the MW, LMC, and SMC)

We include C, O, Mg, Si, S, Cr, Fe, Zn in the calculation of  $D/G$  using Equation 5. However, the full suite of elements that make up most of the dust mass does not necessarily have depletion measurements in nearby galaxies or DLAs. In particular, C and O in the LMC and SMC are not measured because the UV transitions of C and O are either too saturated or too weak. The same issues applies to DLA systems. Unfortunately, C and O constitute the largest mass reservoir of heavy elements that can be included in dust. This limitation can be circumvented thanks to the relative invariance of the collective behavior of depletions observed in the MW, LMC, and SMC (Paper III). As in [Péroux & Howk \(2020\)](#), [Roman-Duval et al. \(2021\)](#) and Paper III, we therefore use the assumption that the relation between C or O depletions and Fe depletions behaves similarly in the Milky Way, LMC, SMC, and DLAs. Knowing the depletions of Fe for all our sight lines, we apply the known MW relation between  $\delta(\text{C})$  or  $\delta(\text{O})$  and  $\delta(\text{Fe})$  (Equation 2 and coefficients in Table 2) from [Jenkins \(2009\)](#) to obtain an estimate of  $\delta(\text{C})$  or  $\delta(\text{O})$  for each DLA or MW, LMC, or SMC sight-line. The error on the  $A_X$  and  $B_X$  coefficients are propagated through the calculation of C and O depletions.

We note that a deficiency of carbon relative to other elements in DLAs ([Cooke et al. 2011](#)), as is the case in the the Magellanic Clouds ( $\log \text{C}/\text{O} = -0.56$  in the LMC versus  $-0.30$  in the MW, and  $-0.62$  in the SMC)

may potentially affect the rate of carbon depletions compared to those of other elements. For example, the fraction of carbonaceous dust and PAHs relative to silicates is different between the MW, LMC, and SMC (Chasnet et al. 2019), which could be attributed to the different chemical affinities of dust compounds induced by the lower carbon abundance in the LMC and SMC, and possibly DLAs compared to the MW.

Furthermore, for some DLA systems, gas-phase abundances were not measured for the full suite of elements used in the computation of D/G, even though depletions can be estimated for all elements from  $[\text{Zn}/\text{Fe}]$ . This is the case for C for all DLAs, O in most DLAs, and other elements in some DLAs. In those cases, we estimated the total abundance of X as  $(X/\text{H}) = (X/\text{H})_{\odot} + \Delta_Z$ , where  $\Delta_Z$  is the error-weighted mean total (depletion corrected) metallicity difference from solar estimated from the measured abundances of other elements:

$$\Delta_Z = \frac{\sum_X \frac{(\frac{X}{\text{H}})_{\text{tot}} - (\frac{X}{\text{H}})_{\odot}}{\sigma(\frac{X}{\text{H}})_{\text{tot}}^2}}{\sum_X \frac{1}{\sigma(\frac{X}{\text{H}})_{\text{tot}}^2}} \quad (7)$$

We provide online binary tables in the fits format containing all gas-phase abundance measurements in the two DLA and sub-DLA samples, as well as our best estimate of the depletions, total abundances, D/G, and D/M obtained following the approach described above. The binary tables are described in more detail in Appendix A.

### 3. D/G VERSUS METALLICITY: THE TENSION BETWEEN DLAS, FIR, AND DEPLETIONS

With estimates of D/G in DLAs obtained from the gas-phase  $[\text{Zn}/\text{Fe}]$  ratio and the relation between  $[\text{Zn}/\text{Fe}]$  and depletions from DC16 (see Section 2.2), we can examine the relation between (total) metallicity and D/G estimated in those systems. We can then compare this relation to 1) the relation obtained from depletions in the MW, LMC, and SMC (Paper III), and 2) the relation observed in nearby galaxies using the FIR to trace dust, 21 cm to trace atomic gas, and CO (1-0) emission to trace molecular gas (Roman-Duval et al. 2017; Rémy-Ruyer et al. 2014; De Vis et al. 2019). These relations between metallicity and D/G are shown in Figure 1. For the LMC and SMC, we plot the integrated D/G from Paper III.

The chemical evolution model tracks from Feldmann (2015) are also shown in Figure 1. This chemical evolution model takes into account dust formation in evolved stars, dust growth in the ISM, dust destruction by SNe shocks, and dust dilution by inflows of pristine gas. In the model, the D/M is high with most metals locked in

the dust-phase above a critical metallicity at which the dust input rate from evolved stars (AGB + supernovae) and ISM dust growth balances the dust destruction by supernova (SN) shockwaves and dilution by inflows of pristine gas. Below this critical metallicity, the D/M is low because the dust input is dominated by stellar sources, as ISM dust growth is not sufficiently efficient to counter the dust destruction and dilution effects. In Figure 1, the model tracks correspond to a plausible range of the parameter  $\gamma$ , which is the ratio of the molecular gas consumption by star-formation timescale (typically 2 Gyr, see Bigiel et al. 2008) to the timescale for dust growth in the ISM in the MW (typically 10 Myr, see Hirashita 2000; Asano et al. 2013; Feldmann 2015).  $\gamma$  ranges from  $2 \times 10^3$  to  $10^6$  with a fiducial value  $\gamma = 3 \times 10^4$  giving the best agreement with the FIR measurements.

As pointed out by Galliano et al. (2018), DLAs and nearby galaxies follow two distinct trends in their D/G versus metallicity. The FIR-based D/G in nearby galaxies (including the LMC and SMC) roughly follows the model tracks from Feldmann (2015), with the D/G dropping non-linearly with decreasing metallicity below a critical metallicity of about 10% — 20% solar. The DLAs follow a much flatter relation, with D/G being almost linear with metallicity. The D/G obtained from depletions in the LMC and SMC, while significantly higher than the FIR-based D/G in those galaxies, is compatible with both trends because the metallicity of the SMC is still high enough that it lies above the critical metallicity at which a large decrease in D/G is theoretically expected.

Paper III proposes that systemic effects associated with D/G measurements obtained from emission-based tracers could explain this discrepancy. Those include the poorly constrained yet variable FIR opacity of dust (Roman-Duval et al. 2014; Stepnik et al. 2003; Demyk et al. 2017; Ysard et al. 2018; Clark et al. 2019), which could account for a systematic uncertainty of a factor of a few; the metallicity-dependent (but not well constrained) CO-to-H<sub>2</sub> conversion factor (Bolatto et al. 2013; Heintz & Watson 2020; Chiang et al. 2021); geometrical effects and differences in the volume of ISM probed between pencil-beam absorption-based measurements and integrated emission-based measurements.

However, it is also possible that some of the assumptions made to infer D/G in DLAs contribute to this discrepancy. First, the computation of D/G in DLAs relies on estimates of the dominant contributions from C and O to the dust budget. C and O can be measured in DLA systems with metallicities low enough that the transitions for these elements are not saturated (Pettini et al.

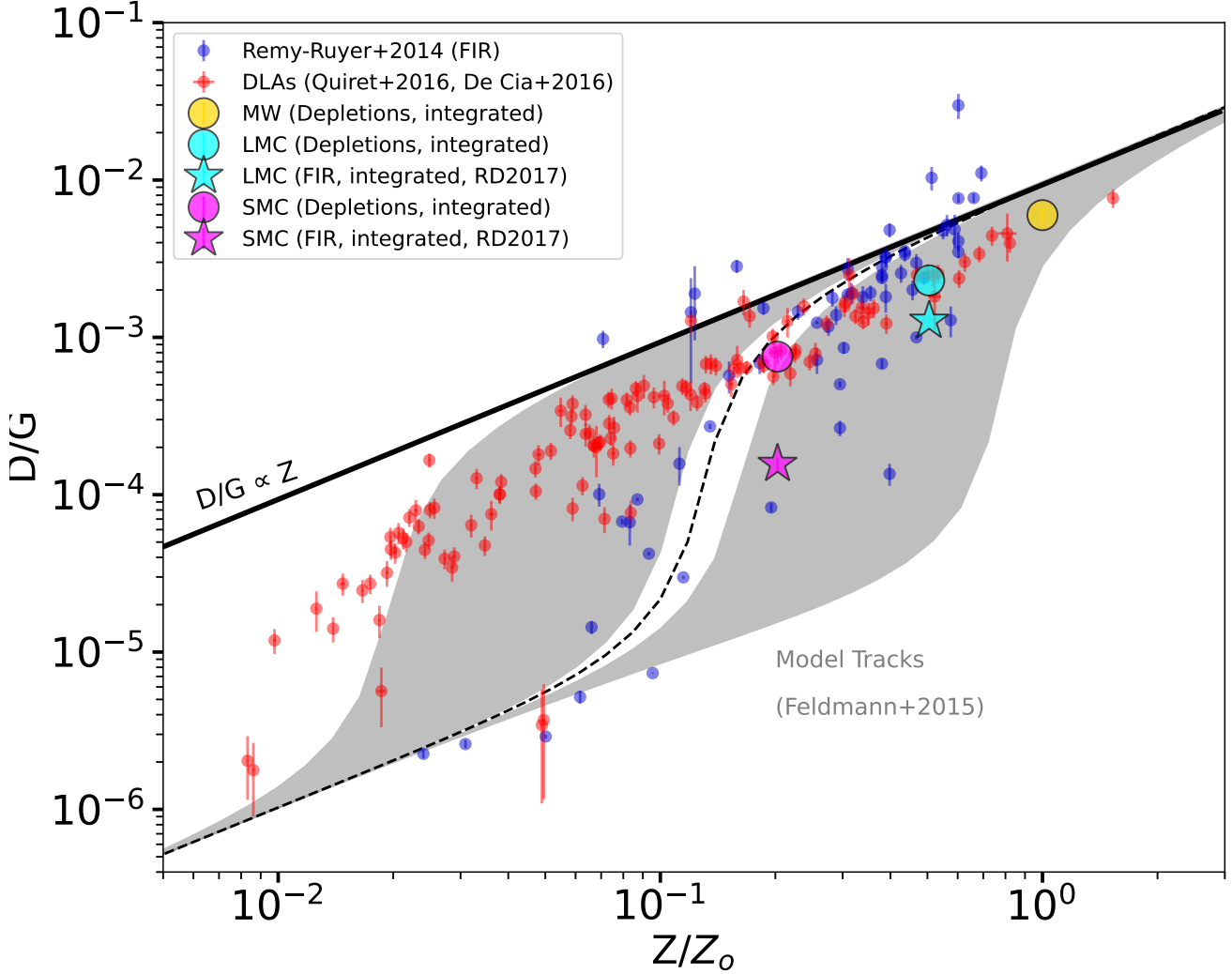


**Figure 1.** Dust-to-gas ratio as a function of total (gas + dust) metallicity in different systems and from different observational methods. The blue points correspond to the D/G measured in nearby galaxies using FIR emission to trace dust, and 21 cm and CO rotational emission to trace atomic and molecular gas (Rémy-Ruyer et al. 2014; De Vis et al. 2019). The cyan and magenta stars correspond to similar measurements in the LMC and SMC, respectively (Roman-Duval et al. 2017). The FIR measurements are integrated (total dust mass/total gas mass). The yellow, cyan and magenta circles show the integrated D/G measurements obtained from spectroscopic depletions in the MW, LMC, and SMC (Jenkins 2009; Roman-Duval et al. 2021; Jenkins & Wallerstein 2017) taken from Paper III. The red circles correspond to D/G estimated in DLAs using the [Zn/Fe] abundance ratio as a tracer of depletions (DC16). Lastly, the gray tracks show the chemical evolution model from Feldmann (2015) for a range of the  $\gamma$  parameter ( $2 \times 10^3 - 10^6$ ).

2008). But for DLA systems with metallicities sufficient to detect the Zn lines, which is key to estimate depletions from [Zn/Fe], the C and O lines are saturated. As a result, estimates of C and O depletions in those systems rely on the MW relation between depletions of different elements, which might not apply at low metallicity due to potentially different abundance ratios and subsequent chemical affinities. Furthermore, the depletions of C and O in the MW are subject to large errors due to the difficulty in measuring them. While this limitation

cannot be addressed with observations, the uncertain contribution of C and O to the dust mass budget should be captured in our error bars.

Second, as described in Section 2.2, the estimation of depletions in DLAs from [Zn/Fe] following the prescriptions presented in DC16 relies on a few fundamental assumptions, which could each potentially contribute to the discrepancy observed in the metallicity-D/G relation between nearby galaxies observed in the FIR and DLAs observed using QSO spectroscopy. Those assump-



tions are that 1) Zn behaves like an iron-peak element in DLAs (i.e.,  $\alpha(\text{Zn}) = 0$ ); 2) the relation between  $[\text{Zn}/\text{Fe}]$  and  $\delta(\text{Zn})$  in the MW is applicable to DLAs; and 3) the relation between  $[\text{Zn}/\text{Fe}]$  and  $\delta(\text{Zn})$  is linear with a zero-intercept (i.e.,  $\delta(\text{Zn}) = 0$  for  $[\text{Zn}/\text{Fe}] = 0$ ).

The assumption that  $\alpha(\text{Zn}) = 0$  is the fundamental underpinning of the estimation of elemental depletions and D/G from the  $[\text{Zn}/\text{Fe}]$  gas-phase abundance ratio. There is, however, a growing body of evidence that Zn may not behave like an iron-peak element at low metallicity, but rather show enhancement of up to 0.5 dex. This has been shown in MW stars (da Silveira et al. 2018; Sitnova et al. 2022) and in the Sculptor galaxy (Skúladóttir et al. 2017). An enhancement of Zn relative to Fe would increase the  $[\text{Zn}/\text{Fe}]$  ratio, and in turn lead to an over-estimation of depletion levels and D/G. In addition to a possible nucleosynthetic enhancement of Zn in low metallicity DLAs, measurements of Zn abundances can be affected by contamination from Cr II and Mg I lines (Jenkins & Wallerstein 2017; Roman-Duval et al. 2021). This is corrected for in abundances measurements in nearby galaxies, but it is unclear if such careful treatment is applied to DLA systems. Contamination by blended lines would also lead to an overestimation of  $[\text{Zn}/\text{Fe}]$ . Nevertheless, while we acknowledge that the possible nucleosynthetic enhancement of Zn in low metallicity systems might be a fundamental flaw of the approach of using  $[\text{Zn}/\text{Fe}]$  as a tracer of depletions in DLAs, the goal of this paper is not to address the validity of this assumption, nor to evaluate its impact on the estimation of D/G in those high redshift systems.

Rather, the depletion measurements obtained in the MW, LMC and SMC discussed in Paper III provide an opportunity to challenge and modify the second and third assumptions above (i.e., the relation between  $[\text{Zn}/\text{Fe}]$  and  $\delta(\text{Zn})$  in the MW is applicable to DLAs; and the relation between  $[\text{Zn}/\text{Fe}]$  and  $\delta(\text{Zn})$  is linear with a zero-intercept), and examine whether perturbing these assumptions can help resolve the discrepancy observed in the metallicity-D/G relation between nearby galaxies (based on FIR) and DLAs (based on  $[\text{Zn}/\text{Fe}]$ ). Specifically, in the rest of this paper, we derive the relation between  $[\text{Zn}/\text{Fe}]$  and depletions in each of the MW, LMC and SMC based on the depletion samples from Paper III, and apply these relations to DLAs systems. We then examine the relation between metallicity and D/G in DLAs derived with each of these "calibrations" of the  $[\text{Zn}/\text{Fe}]$ -depletion relation.

#### 4. CALIBRATING THE RELATION BETWEEN $[\text{Zn}/\text{Fe}]$ AND DEPLETIONS IN THE MW, LMC AND SMC

Abundance ratios are heavily influenced by the different rates of depletion for the elements involved (see Equation 3). Therefore, comparing the relations between different abundance ratios in the MW, LMC, SMC, and DLAs can reveal key information about the depletion process in those systems, and in particular whether those relations vary from system to system and/or with total metallicity. Applying calibrations of the  $[\text{Zn}/\text{Fe}]$ -depletion relation based on MW, LMC, and SMC measurements to DLAs requires those relations between abundance ratios to be invariant. We verify that this is a valid assumption in Section 4.1. We focus on the relation between  $[\text{Zn}/\text{Fe}]$  and other abundance ratios, since  $[\text{Zn}/\text{Fe}]$  is used as a tracer of depletions in many DLA studies. In Section 4.2, we then derive the relation between  $[\text{Zn}/\text{Fe}]$  and depletions in the MW, LMC, and SMC.

##### 4.1. Comparison of abundance ratios in the MW, LMC, SMC, and DLAs

We first examine the relation between  $[\text{Zn}/\text{Fe}]$  and other abundance ratios in the MW, LMC, SMC, and DLAs in Figures 2 and 3. Figure 2 includes abundance ratios  $[\text{X}/\text{Zn}]$  with  $\text{X} = \text{Mg}, \text{Si}, \text{S}, \text{Cr}$ , while Figure 3 includes abundance ratios  $[\text{X}/\text{S}]$  with  $\text{X} = \text{Mg}, \text{Si}, \text{Zn}, \text{Fe}, \text{Cr}$ . This is similar to the comparison performed by De Cia (2018), but with the addition of the new LMC sample obtained from the METAL program (Roman-Duval et al. 2019, 2021). For the MW, LMC, and SMC, both the abundance ratios toward individual sight-lines and the relations derived from the  $A$ ,  $B$ , and  $z$  coefficients relating depletions and  $F_*$  (and hence relating depletions of different elements) are shown in Figures 2 and 3 (see Section 2.1, Equation 2, and Table 2). We note that, while plotted as independent (orthogonal) in  $x$  and  $y$ , error bars in Figure 2 should not be orthogonal since Zn abundances are involved in both axes.

As shown in Paper III, the relations between abundance ratios derived from the  $A_X$ ,  $B_X$ , and  $z_X$  coefficients are not simple linear functions due to depletions being capped at a value of zero. The abundance ratio  $[\text{X}/\text{Y}]$  is determined by the depletions and  $\alpha$ -enhancement of X and Y via Equation 3. In Equation 3, the depletion of X or Y is  $\delta(\text{X}) = A_X(F_* - z_X) + B_X$  and  $\delta(\text{X})$  is capped at zero value. This results in  $[\text{X}/\text{Y}]$  following the piece-wise linear functions shown in Figure 2 and 3 in the MW, LMC, and SMC.

The relations between  $[\text{Zn}/\text{Fe}]$  and  $[\text{X}/\text{Zn}]$  in Figure 2 are generally tight and in reasonable agreement between the MW, LMC, SMC, and DLAs, even for the lowest metallicity DLAs (as traced by their gas-phase  $[\text{Zn}/\text{H}]$ ,

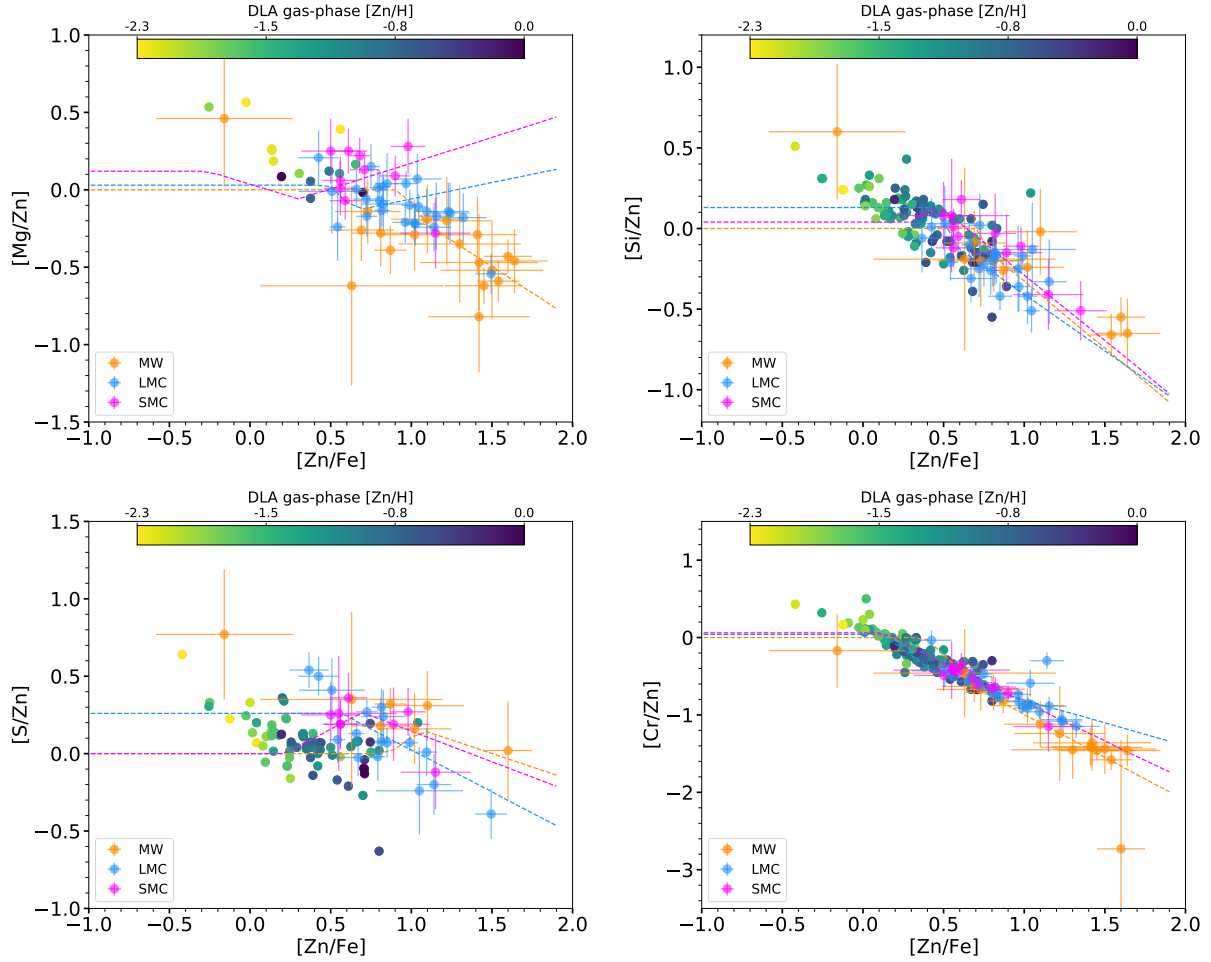


**Figure 2.** Relation between  $[Zn/Fe]$  and other abundance ratios ( $[X/Zn]$  with  $X = Mg, Si, S, Fe, Cr$ ) in the MW (orange), LMC (blue), SMC (magenta) and DLAs (points with color scale). The dashed lines are obtained from the relation between depletions of different elements in the MW, LMC, and SMC (see Equation 2 and Table 2). The DLA points have a color scaled by gas-phase  $[Zn/H]$ , an approximate tracer of total metallicity since Zn is not severely depleted

which should be an approximate indicator of the total metallicity since Zn is lightly depleted). However, a few mild deviations are worth noting. First, the relation between  $[Zn/Fe]$  and  $[Mg/Zn]$  or  $[Mg/S]$  obtained from the  $A_X$ ,  $B_X$ , and  $z_X$  coefficients differs between the MW, LMC, and SMC. This is due to a combination of effects. First, Mg, S, and Zn deplete at approximately the same rate in the LMC and SMC (see Figure 1 in paper III), implying that the relation between  $[Mg/S]$  or  $[Mg/Zn]$  as a function of  $[Zn/Fe]$  should be fairly flat. In practice, the limited dynamic range of the measurements introduces uncertainties in the fitted linear relations. This is particularly an issue for Mg in the SMC, where, owing to the paucity of measurements, the  $A_{Mg}$  slope is determined with a S/N of 1 ( $0.25 \pm 0.26$ , see Jenkins & Wallerstein (2017) and Table 2). These large uncertainties lead to fluctuations in the piece-wise linear functions describing the relations between  $[Zn/Fe]$  and  $[X/Zn]$ , with the

linear extrapolation beyond the measurements diverging upward for the SMC (and to a lesser extent the LMC). Nevertheless, the abundance ratio measurements toward individual sight-lines in the MW, LMC, SMC, and DLAs follow a fairly tight linear relation.

Second, DLAs with the lowest  $[Zn/Fe]$  ratios and metallicities (traced by the gas  $[Zn/H]$ ) tend to exhibit  $[Mg/Zn]$  and  $[Si/Zn]$  ratios that are higher by up to 0.5 dex compared to the extrapolations from the MW, LMC, and SMC relations. This could be attributed to mild  $\alpha$ -enhancement in the lowest metallicity systems (as traced by the gas-phase  $[Zn/H]$ ), which also have the lowest  $[Zn/Fe]$  ratios (see for example Rafelski et al. 2012).

Third, there might be tentative hints of  $\alpha$ -enhancement for Zn in the top right panel of Figure 3, showing  $[Si/S]$  as a function of  $[Zn/Fe]$ . Because Si and S are both  $\alpha$ -elements,  $[Si/S] \sim 0$  (solar ratio) indicates no dust depletion effects in those elements. In

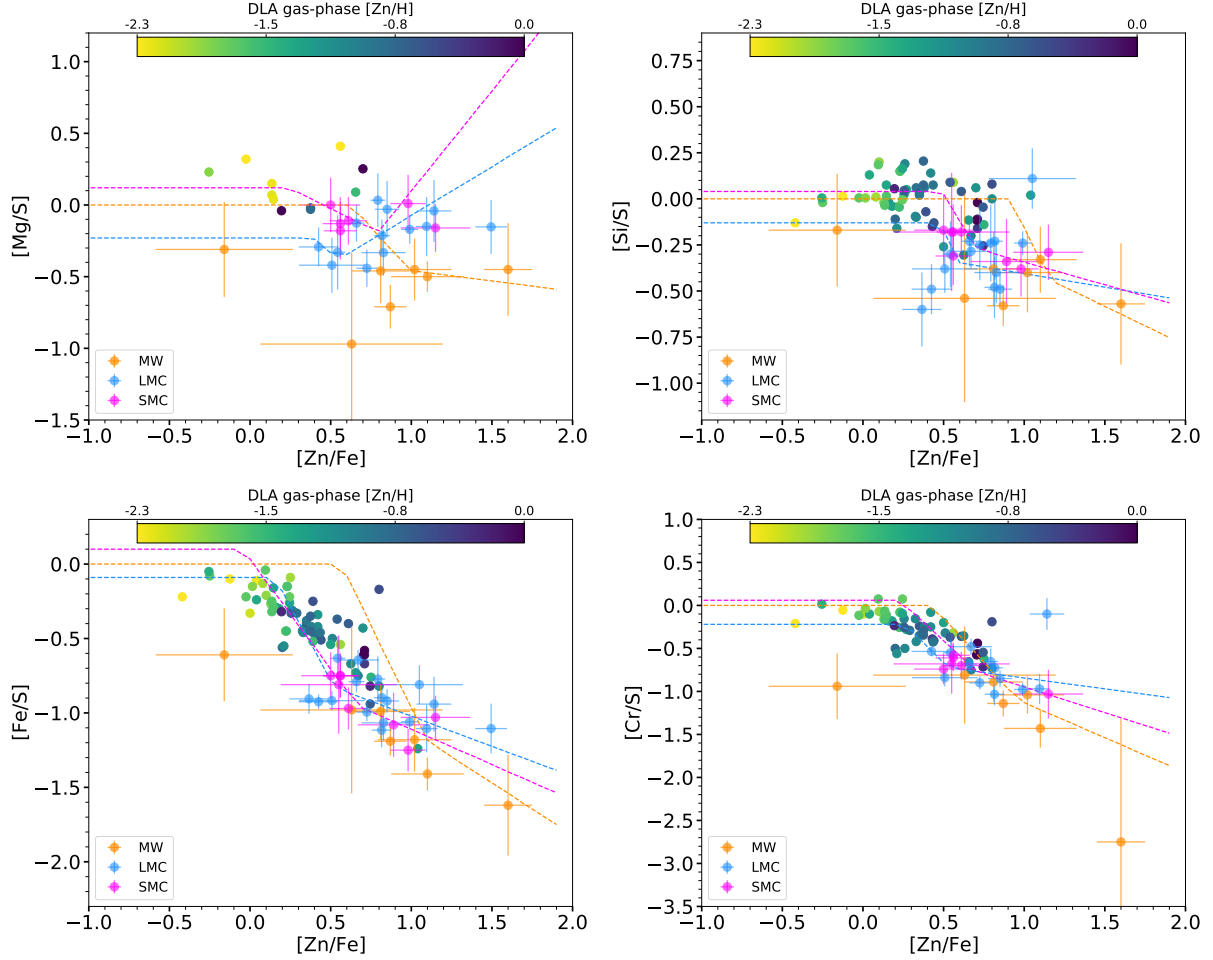


**Figure 3.** Relation between  $[\text{Zn}/\text{Fe}]$  and other abundance ratios  $[X/\text{S}]$  with  $X = \text{Mg}, \text{Si}, \text{Zn}, \text{Fe}, \text{Cr}$  in the MW (orange), LMC (blue), SMC (magenta) and DLAs (points with color scale). The dashed lines are obtained from the relation between depletions of different elements in the MW, LMC, and SMC (see Equation 2 and Table 2). The DLA points have a color scaled by gas-phase  $[\text{Zn}/\text{H}]$ , an approximate tracer of total metallicity since Zn is not severely depleted.

the MW, LMC, and SMC, Si and S are not depleted below  $[\text{Zn}/\text{Fe}] = 0.6$  (Fe is still depleted at the 0.6 dex level when Si and S reach zero depletion values). So, one would expect  $[\text{Si}/\text{S}] \sim 0$  for  $[\text{Zn}/\text{Fe}] < 0.6$  if DLAs follow the MW, LMC and SMC. Yet, there are a number of DLA systems with  $[\text{Si}/\text{S}] \sim 0$  and a  $[\text{Zn}/\text{Fe}]$  ratio in the range 0.6 to 1. Those systems have gas-phase metallicities  $[\text{Zn}/\text{H}]$  in the range  $-1$  to  $-0.5$  (except for one system with solar metallicity). This enhancement of  $[\text{Zn}/\text{Fe}]$  in DLAs un-depleted in Si could result from a nucleosynthetic enhancement of Zn by up to 0.4 dex, consistent with measurements in low metallicity red giants (da Silveira et al. 2018). This evidence is very tentative given the difficulty in robustly discerning signs of  $\alpha$ -enhancement owing to the large scatter. In particular, the high  $[\text{Zn}/\text{Fe}]$  ratio in those systems could be due to Fe being more depleted than in nearby galaxies when Si is not depleted. We also note the caveat that the neu-

tral gas abundances of S in the MW, LMC, and SMC that are the basis for this comparison may be slightly contaminated by S II residing in ionized gas (Jenkins 2009, , see below), which would bias  $[\text{Si}/\text{S}]$  low in those galaxies.

Last,  $[\text{S}/\text{Zn}]$  in the MW, LMC, and SMC is enhanced compared to DLAs, which is likely due to mild contamination from S II in ionized gas. Ionized gas can originate in the H II region surrounding the background massive star, as pointed out by Jenkins (2009) and Jenkins & Wallerstein (2017), or in the diffuse ionized medium. This effect can artificially increase the abundance of S inferred in a sight-line by normalizing the S II column density to the HI column density, i.e., under the assumption that S II absorption only stems from atomic gas. This effect can occur for S because the ionization potential of S is lower than that of H, making S II the dominant ion in the ISM, but the ionization potential

of  $S^+$  is high enough (23.4 eV) that very few photons from the background star can ionize  $S^+$ . As a result,  $S\ II$  is also the dominant ion in ionized gas, and could contribute a significant amount to the  $S\ II$  column density along the sight-line, for which we can only measure  $H\ I$ . This effect may not impact abundances in DLAs as significantly because the sight line just passes through a random part of a foreground neutral system and does not necessarily penetrate an  $H\ II$  region. The  $S\ II$  abundance measured in the MW, LMC, and SMC would subsequently appear to be enhanced in those galaxies compared to DLAs. We note that, principle, diffuse ionized gas in DLAs could also contribute to this effect, but to a lesser extent.

Given these relatively subtle differences in the relations between  $[Zn/Fe]$  and other abundance ratios between the MW, LMC, SMC, and DLAs, calibrations of depletions as a function of  $[Zn/Fe]$  established in the MW, LMC, and SMC should be reasonably applicable to DLA systems.

Nevertheless, we caution that DLAs where Zn is not detectable are not included in this sample. These DLAs likely have very low metallicities, and the applicability of the depletion calibrations derived here cannot be tested in those systems.

#### 4.2. Calibration of depletions as a function of $[Zn/Fe]$ in the MW, LMC and SMC

Having demonstrated that the calibration of the relation between  $[Zn/Fe]$  and depletions established in the MW, LMC, or SMC should reasonably be applied to DLAs, we now proceed with deriving those calibrations. We proceed numerically using a look-up table, since an analytical description of the piecewise linear functions relating abundance ratios would be too complex to describe. The method is as follows.

- We first create an array of  $F_*$  values ranging from  $-1.5$  to  $2.5$  (which covers the entire range exhibited by local galaxies and DLAs). For each  $F_*$  value in the array, we compute the depletions of all elements using Equation 2 and the coefficients  $A_X$ ,  $B_X$ , and  $z_X$  given in Table 2 for each of the MW, LMC, and SMC. For some elements (e.g., C, O), depletions were not measured in the LMC and SMC. In those cases, we circumvent this lim-

itation using the same method as described in Section 2.4. We use the MW relation between  $\delta(X)$  and  $\delta(Fe)$  to estimate the depletion of C or O from the depletion of Fe computed for each  $F_*$  value in the grid and each galaxy.

- We cap the depletions at a value of zero.
- We deduce the gas-phase  $[Zn/Fe]$  for each  $F_*$  grid point from the depletions of Zn and Fe and Equation 3. We use the stellar abundances of Zn and Fe given in Table 1 to compute  $\alpha(Zn)$  and  $\alpha(Fe)$  in the LMC and SMC (recall  $\alpha(X) = [X/Fe]$  in young stars and  $\alpha = 0$  in the MW).

This procedure provides us with a grid of  $F_*$ , depletions for all elements, and  $[Zn/Fe]$  values for each galaxy (MW, LMC, SMC), from which we tabulate the relation between gas-phase  $[Zn/Fe]$  and depletions of all elements. Those relations are shown in Figure 4 (dashed lines) and are given in Tables 3, 4, and 5 for the MW, LMC, and SMC, respectively. The uncertainty on those relations shown in Figure 4 is computed using a Monte Carlo approach, by propagating the uncertainty on the  $A_X$  and  $B_X$  coefficients used to derive those relations. Figure 4 also shows the depletion measurements as a function of  $[Zn/Fe]$  toward individual sight-lines in the MW, LMC, and SMC.

The relation between  $[Zn/Fe]$  and depletions established here relies on the fits between depletions of different elements or  $F_*$ , which are determined with relatively high accuracy and robustness. However,  $[Zn/Fe]$  basically corresponds to the difference between the depletions of Zn and Fe (Equation 3), which combines the errors on the Zn and Fe measurements. As a result, the relation between  $[Zn/Fe]$  and depletions shown in Figure 4 exhibits substantial scatter, consistent with the error on  $[Zn/Fe]$ . It is therefore important to evaluate the performance of the calibration of the  $[Zn/Fe]$ — $\delta(X)$  relation by applying it to the individual  $[Zn/Fe]$  measurements in each of the MW, LMC, and SMC, and compare the resulting depletions estimated from  $[Zn/Fe]$  to the actual depletion measurements. The results of this comparison are included in Appendix B, and show that the scatter between depletions derived from gas-phase and stellar abundances and those inferred from  $[Zn/Fe]$  and various calibrations (DC16, MW, LMC, SMC) is considerably larger than the typical uncertainties on gas-phase abundance measurements.

#### 4.3. Comparison with the De Cia et al. (2016) calibration

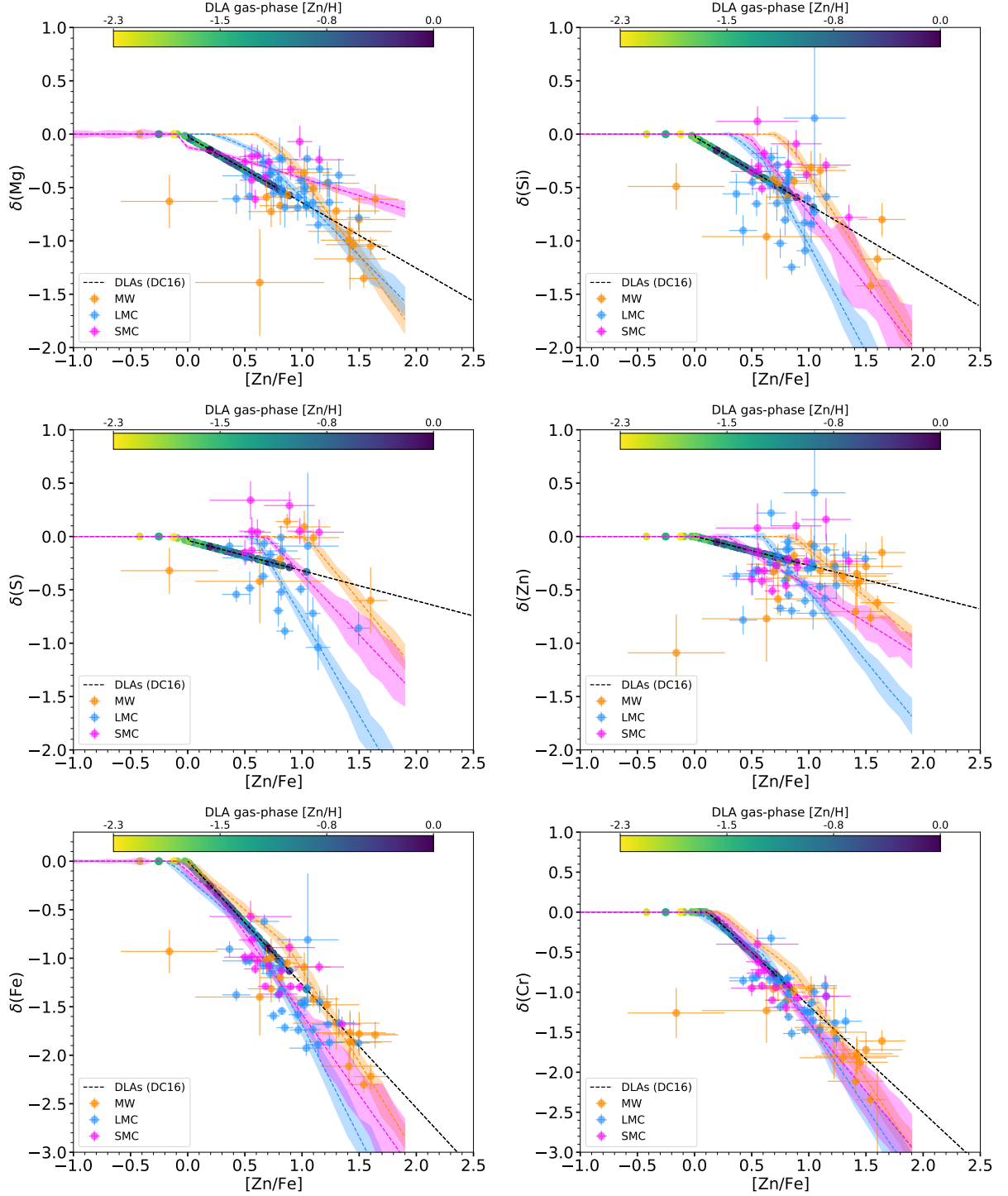


**Figure 4.** Depletions as a function of the  $[Zn/Fe]$  abundance ratio measured in the MW (orange), LMC (blue), and SMC (magenta). The dashed lines are obtained from the relation between depletions of different elements in the MW, LMC, and SMC (see Equation 2 and Table 2). The uncertainties shown as bands are computed from a Monte Carlo approach to propagate the uncertainties on the  $A_X$  and  $B_X$  coefficients used to derive the relations. The DLAs are plotted as points with color scaled by gas-phase  $[Zn/H]$ , an approximate tracer of total metallicity since Zn is not severely depleted. In DLAs, the depletions are inferred from  $[Zn/Fe]$  using the linear calibrations presented in De Cia et al. (2016).

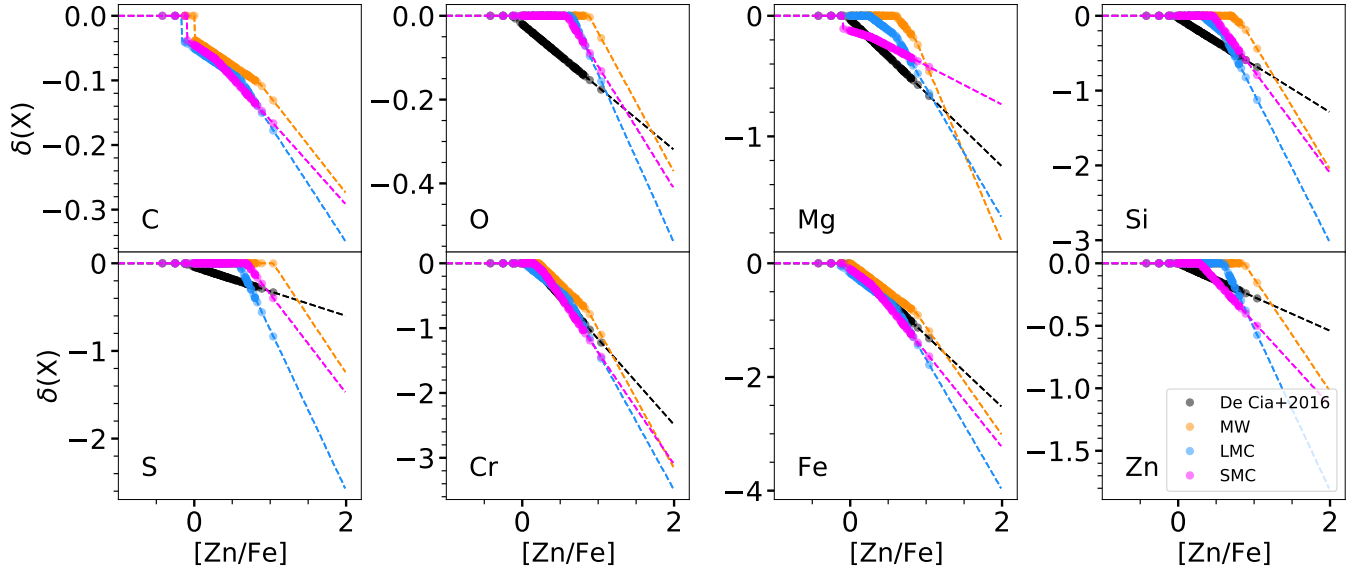


**Figure 5.** Relation between  $[Zn/Fe]$  and depletions established in the MW (orange lines), LMC (blue lines) and SMC (magenta lines). The relation derived in De Cia et al. (2016) is also plotted for comparison (black lines). The corresponding depletion estimates obtained from Equation 4 applied to the De Cia et al. (2016) and Quiret et al. (2016) DLA samples are plotted as points.

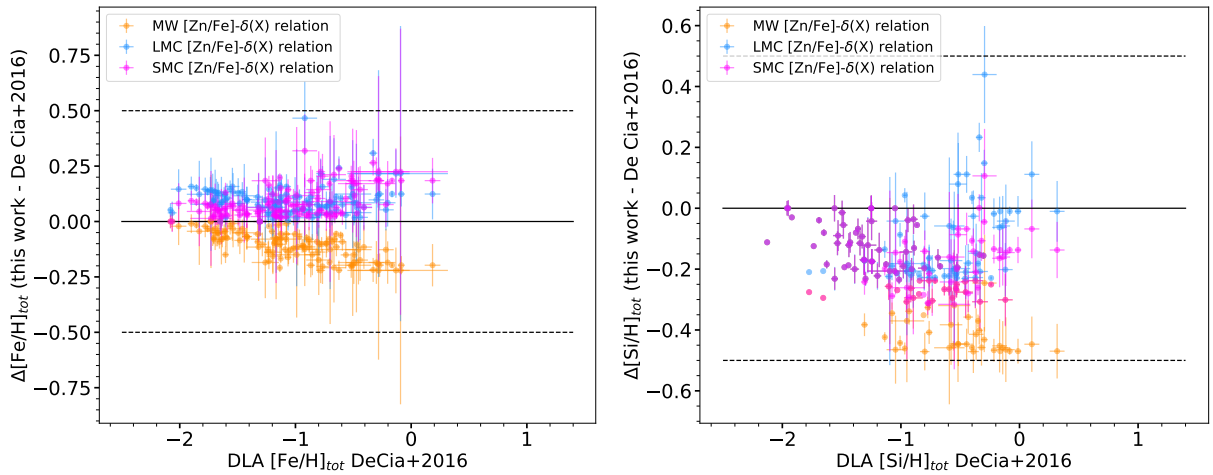


**Figure 6.** Comparison of the total, depletion-corrected, Fe (left) and Si (right) metallicities ( $[Fe/H]_{tot}$  and  $[Si/H]_{tot}$ ) in DLAs inferred using the relation between  $[Zn/Fe]$  and depletions derived in De Cia et al. (2016) (see Equation 4) and from the  $[Zn/Fe]$ —depletion relation observed in the MW, LMC, or SMC. The solid black line indicates a 1:1 correspondence, while the dashed line indicate  $\pm 0.5$  dex differences.

**Table 3.** Numerical relation between  $[\text{Zn}/\text{Fe}]$  and depletions of C, O, Mg, Si, S, Ti, Cr, Fe, Ni, Zn derived in the MW

$[\text{Zn}/\text{Fe}]$	$\delta(\text{C})$	$\delta(\text{O})$	$\delta(\text{Mg})$	$\delta(\text{Si})$	$\delta(\text{S})$	$\delta(\text{Ti})$	$\delta(\text{Cr})$	$\delta(\text{Fe})$	$\delta(\text{Ni})$	$\delta(\text{Zn})$
-0.50	0.00	0.00	0.00	0.00	0.00	0.00	0.00	0.00	0.00	0.00
-0.40	0.00	0.00	0.00	0.00	0.00	0.00	0.00	0.00	0.00	0.00
-0.30	0.00	0.00	0.00	0.00	0.00	0.00	0.00	0.00	0.00	0.00
-0.20	0.00	0.00	0.00	0.00	0.00	0.00	0.00	0.00	0.00	0.00
-0.10	0.00	0.00	0.00	0.00	0.00	0.00	0.00	0.00	0.00	0.00
-0.00	0.00	0.00	0.00	0.00	0.00	0.00	0.00	0.00	0.00	0.00
0.10	-0.05	0.00	0.00	0.00	0.00	0.00	0.00	-0.10	0.00	0.00
0.20	-0.05	0.00	0.00	0.00	0.00	0.00	0.00	-0.21	-0.07	0.00
0.30	-0.06	0.00	0.00	0.00	0.00	-0.03	-0.09	-0.30	-0.18	0.00
0.40	-0.07	0.00	0.00	0.00	0.00	-0.20	-0.21	-0.40	-0.30	0.00
0.50	-0.08	0.00	0.00	0.00	0.00	-0.36	-0.32	-0.50	-0.41	0.00
0.60	-0.08	0.00	-0.00	0.00	0.00	-0.52	-0.44	-0.60	-0.53	0.00
0.70	-0.09	0.00	-0.07	0.00	0.00	-0.67	-0.54	-0.69	-0.64	0.00
0.80	-0.10	0.00	-0.15	-0.09	0.00	-0.83	-0.65	-0.80	-0.76	0.00
0.90	-0.11	-0.01	-0.25	-0.20	0.00	-1.04	-0.80	-0.93	-0.91	-0.03
1.00	-0.13	-0.04	-0.40	-0.37	0.00	-1.34	-1.02	-1.12	-1.13	-0.12
1.10	-0.14	-0.07	-0.55	-0.54	-0.08	-1.65	-1.23	-1.31	-1.35	-0.21
1.20	-0.16	-0.11	-0.70	-0.71	-0.21	-1.96	-1.45	-1.50	-1.58	-0.30
1.30	-0.17	-0.14	-0.85	-0.88	-0.34	-2.26	-1.67	-1.70	-1.80	-0.39
1.40	-0.18	-0.17	-0.99	-1.04	-0.47	-2.55	-1.87	-1.88	-2.01	-0.48
1.50	-0.20	-0.21	-1.14	-1.21	-0.60	-2.86	-2.09	-2.07	-2.23	-0.57
1.60	-0.21	-0.24	-1.29	-1.38	-0.73	-3.17	-2.30	-2.26	-2.46	-0.66
1.70	-0.23	-0.27	-1.44	-1.55	-0.86	-3.47	-2.52	-2.45	-2.68	-0.75
1.80	-0.25	-0.31	-1.59	-1.72	-1.00	-3.78	-2.74	-2.65	-2.90	-0.85
1.90	-0.26	-0.34	-1.74	-1.89	-1.13	-4.09	-2.96	-2.84	-3.13	-0.94

NOTE—This table is also available online in machine-readable format with a finer sampling in  $[\text{Zn}/\text{Fe}]$

In Figure 4, we also compare the relation between  $[\text{Zn}/\text{Fe}]$  and depletions in the MW, LMC, and SMC with that inferred in DLAs using Equation 4, taken from DC16. While the the  $[\text{Zn}/\text{Fe}] - \delta(\text{X})$  relations for refractory elements (Fe, Cr) are roughly consistent between the MW, LMC, SMC, and DC16 calibrations, Figure 4 suggests that there are significant differences between these  $[\text{Zn}/\text{Fe}] - \delta(\text{X})$  calibrations for volatile elements (Mg, S, Si, Zn). Indeed, the MW, LMC and SMC calibrations have steeper slopes that are topped at zero, while the DC16 calibrations are linear relations all the way down to low  $[\text{Zn}/\text{Fe}]$ . This results in the depletion levels of volatile elements being much higher (depletions much more negative) with the DC16 calibration compared to the MW, LMC, or SMC calibrations.

The main reason for this difference stems from the difference in methodology and formalism used to de-

rive these relations, and in particular on the assumed shape of the curve of depletions vs  $[\text{Zn}/\text{Fe}]$  as depletions approach zero. On the one hand, the MW, LMC, and SMC relations between  $[\text{Zn}/\text{Fe}]$  and  $\delta(\text{X})$  shown in Figure 4 are based on Equation 2 and associated  $A_X$ ,  $B_X$ , and  $z_X$  coefficients linking depletions of different elements (see Table 2). On the other hand, the linear relation from DC16 described by the  $A_2$  and  $B_2$  coefficients in Equation 4 relies on 1) linear fits to abundance ratios  $[\text{X}/\text{Zn}]$  vs  $[\text{Zn}/\text{Fe}]$  in DLAs, and 2) a linear fit with zero-intercept to MW measurements of  $\delta(\text{Zn})$  as a function of  $[\text{Zn}/\text{Fe}]$  (see Section 2.2). Figures 2 and 3 show that the relation between abundance ratios are not significantly different between the MW, LMC, SMC, and DLAs, such that the fits of  $[\text{X}/\text{Zn}]$  to  $[\text{Zn}/\text{Fe}]$  in DLAs (point #1 above) should not contribute much of the difference seen between calibrations in Figure 4.

**Table 4.** Numerical relation between  $[\text{Zn}/\text{Fe}]$  and depletions of Mg, Si, S, Ti, Cr, Fe, Ni, Zn derived in the LMC

$[\text{Zn}/\text{Fe}]$	$\delta(\text{Mg})$	$\delta(\text{Si})$	$\delta(\text{S})$	$\delta(\text{Ti})$	$\delta(\text{Cr})$	$\delta(\text{Fe})$	$\delta(\text{Ni})$	$\delta(\text{Zn})$
-0.50	0.00	0.00	0.00	0.00	0.00	0.00	0.00	0.00
-0.40	0.00	0.00	0.00	0.00	0.00	0.00	0.00	0.00
-0.30	0.00	0.00	0.00	0.00	0.00	0.00	0.00	0.00
-0.20	0.00	0.00	0.00	0.00	0.00	0.00	0.00	0.00
-0.10	0.00	0.00	0.00	-0.02	0.00	-0.06	0.00	0.00
-0.00	0.00	0.00	0.00	-0.14	0.00	-0.17	-0.04	0.00
0.10	0.00	0.00	0.00	-0.25	-0.07	-0.27	-0.14	0.00
0.20	0.00	0.00	0.00	-0.37	-0.17	-0.37	-0.24	0.00
0.30	-0.03	0.00	0.00	-0.49	-0.26	-0.48	-0.35	0.00
0.40	-0.07	-0.07	0.00	-0.59	-0.34	-0.57	-0.44	0.00
0.50	-0.12	-0.16	0.00	-0.71	-0.44	-0.67	-0.54	0.00
0.60	-0.17	-0.24	-0.03	-0.83	-0.53	-0.77	-0.64	-0.00
0.70	-0.27	-0.44	-0.21	-1.10	-0.75	-1.00	-0.88	-0.13
0.80	-0.38	-0.65	-0.39	-1.36	-0.96	-1.23	-1.11	-0.26
0.90	-0.49	-0.85	-0.58	-1.63	-1.17	-1.47	-1.34	-0.39
1.00	-0.59	-1.04	-0.75	-1.88	-1.37	-1.68	-1.56	-0.52
1.10	-0.70	-1.24	-0.94	-2.15	-1.59	-1.92	-1.79	-0.65
1.20	-0.81	-1.44	-1.12	-2.41	-1.80	-2.15	-2.02	-0.78
1.30	-0.92	-1.64	-1.31	-2.68	-2.01	-2.38	-2.25	-0.91
1.40	-1.03	-1.84	-1.49	-2.95	-2.23	-2.61	-2.49	-1.04
1.50	-1.14	-2.04	-1.68	-3.21	-2.44	-2.84	-2.72	-1.17
1.60	-1.25	-2.24	-1.86	-3.48	-2.65	-3.07	-2.95	-1.30
1.70	-1.36	-2.44	-2.04	-3.75	-2.87	-3.30	-3.18	-1.43
1.80	-1.46	-2.63	-2.22	-4.00	-3.07	-3.52	-3.40	-1.55
1.90	-1.57	-2.83	-2.40	-4.26	-3.28	-3.75	-3.63	-1.68

NOTE—This table is also available online in machine-readable format with a finer sampling in  $[\text{Zn}/\text{Fe}]$

For refractory elements (Fe, Cr), this relation between  $[\text{X}/\text{Zn}]$  and  $[\text{Zn}/\text{Fe}]$  (point #1 above) dominates the calibration of  $\delta(\text{X})$  vs  $[\text{Zn}/\text{Fe}]$ . Since this relation between  $[\text{X}/\text{Zn}]$  and  $[\text{Zn}/\text{Fe}]$  does not vary significantly between systems, the  $[\text{Zn}/\text{Fe}]$ — $\delta(\text{X})$  relation is not significantly different between the MW, LMC, SMC, and DC16 calibrations as a result.

However, for volatile elements such as Mg, S, Si, Zn, the linear relation with zero intercept between  $\delta(\text{Zn})$  vs  $[\text{Zn}/\text{Fe}]$  assumed in the DC16 depletion calibrations (point #2 above) has a dominant influence on the estimate of  $\delta(\text{X})$  as a function of  $[\text{Zn}/\text{Fe}]$ . This is because  $[\text{X}/\text{Zn}]$  for volatile elements is closer to zero and their depletions are closer to that of Zn. As a result, the effects of the assumed linear function with zero intercept between  $[\text{Zn}/\text{Fe}]$  and  $\delta(\text{Zn})$  are directly reflected on the DC16 curves shown in Figure 4. Indeed, in Figure

4, the slopes of the depletions vs  $[\text{Zn}/\text{Fe}]$  relations are shallower for the DC16 calibrations with close to zero-intercept, similar to Figure 5 of DC16, while the slopes for the MW, LMC and SMC calibrations of depletions vs.  $[\text{Zn}/\text{Fe}]$  are steeper, with a more positive intercept in  $[\text{Zn}/\text{Fe}]$  at  $\delta(\text{X}) = 0$ . The positive intercept in  $[\text{Zn}/\text{Fe}]$  for the MW, LMC and SMC calibrations is explained by the formalism used to derive those calibrations. Indeed, assuming that the relation between depletions of different elements is linear even at low depletions,  $\delta(\text{Zn})$  reaches zero level when  $\delta(\text{Fe})$  is still negative, and therefore  $[\text{Zn}/\text{Fe}]$  is still positive, because a)  $[\text{Zn}/\text{Fe}] = \delta(\text{Zn}) - \delta(\text{Fe})$  (assuming Zn is not  $\alpha$ -enhanced, see Equation 3), and b) that Fe is always more depleted than Zn, meaning  $\delta(\text{Fe})$  is much more negative than  $\delta(\text{Zn})$  (see Figure 1 of paper III). This results in a positive range of  $[\text{Zn}/\text{Fe}]$  for which  $\delta(\text{Zn})$  remains maxed at a value of



**Table 5.** Numerical relation between  $[\text{Zn}/\text{Fe}]$  and depletions of Mg, Si, S, Ti, Cr, Fe, Ni, Zn derived in the SMC

$[\text{Zn}/\text{Fe}]$	$\delta(\text{Mg})$	$\delta(\text{Si})$	$\delta(\text{S})$	$\delta(\text{Ti})$	$\delta(\text{Cr})$	$\delta(\text{Fe})$	$\delta(\text{Ni})$	$\delta(\text{Zn})$
-0.50	0.00	0.00	0.00	0.00	0.00	0.00	0.00	0.00
-0.40	0.00	0.00	0.00	0.00	0.00	0.00	0.00	0.00
-0.30	0.00	0.00	0.00	0.00	0.00	0.00	0.00	0.00
-0.20	0.00	0.00	0.00	0.00	0.00	0.00	0.00	0.00
-0.10	0.00	0.00	0.00	0.00	0.00	0.00	0.00	0.00
-0.00	-0.12	0.00	0.00	0.00	0.00	-0.10	0.00	0.00
0.10	-0.14	0.00	0.00	-0.11	0.00	-0.21	-0.09	0.00
0.20	-0.16	0.00	0.00	-0.22	-0.05	-0.30	-0.19	0.00
0.30	-0.18	0.00	0.00	-0.35	-0.17	-0.41	-0.32	-0.01
0.40	-0.22	0.00	0.00	-0.54	-0.34	-0.58	-0.50	-0.08
0.50	-0.25	-0.06	0.00	-0.72	-0.51	-0.74	-0.69	-0.14
0.60	-0.28	-0.19	0.00	-0.91	-0.68	-0.91	-0.87	-0.21
0.70	-0.31	-0.33	-0.01	-1.10	-0.86	-1.08	-1.05	-0.28
0.80	-0.35	-0.47	-0.13	-1.29	-1.03	-1.24	-1.24	-0.34
0.90	-0.38	-0.60	-0.24	-1.48	-1.20	-1.41	-1.42	-0.41
1.00	-0.41	-0.74	-0.35	-1.67	-1.38	-1.58	-1.60	-0.47
1.10	-0.44	-0.88	-0.47	-1.85	-1.55	-1.74	-1.79	-0.54
1.20	-0.48	-1.01	-0.58	-2.04	-1.72	-1.91	-1.97	-0.61
1.30	-0.51	-1.15	-0.69	-2.23	-1.89	-2.07	-2.15	-0.67
1.40	-0.54	-1.29	-0.81	-2.42	-2.07	-2.24	-2.34	-0.74
1.50	-0.57	-1.42	-0.92	-2.61	-2.24	-2.41	-2.52	-0.81
1.60	-0.61	-1.56	-1.03	-2.80	-2.41	-2.57	-2.70	-0.87
1.70	-0.64	-1.69	-1.15	-2.99	-2.59	-2.74	-2.89	-0.94
1.80	-0.67	-1.83	-1.26	-3.17	-2.76	-2.91	-3.07	-1.00
1.90	-0.70	-1.97	-1.37	-3.36	-2.93	-3.07	-3.25	-1.07

NOTE—This table is also available online in machine-readable format with a finer sampling in  $[\text{Zn}/\text{Fe}]$ 

zero for the MW, LMC, and SMC calibrations, as shown in Figure 5 of DC16 and also Figure 4.

As a consequence, the depletions inferred from the MW, LMC, or SMC calibrations for volatile elements are generally less negative than the depletions inferred from the DC16 calibration in the range of  $[\text{Zn}/\text{Fe}]$  typical of DLA systems ( $[\text{Zn}/\text{Fe}] < 1$ ). In other words, the black line corresponding to the DC16 calibration in Figure 4 lies lower than the orange, blue and magenta lines corresponding to the MW, LMC, and SMC calibrations in the range of  $[\text{Zn}/\text{Fe}]$  occupied by DLAs. Conversely, for  $[\text{Zn}/\text{Fe}]$  values greater than the value of  $\sim 1$  where the DC16 calibration (black) in Figure 4 crosses the MW (orange), LMC (blue), and SMC (magenta) calibrations, depletions inferred from the local calibrations are more negative than those obtained from the DC16 calibration. This high  $[\text{Zn}/\text{Fe}]$  range typically corresponds to higher

metallicity DLA systems. As we will see in the rest of this paper, this has important implications for the D/G and D/M derived from different calibrations. From the less negative depletions with the local calibrations (MW, LMC, SMC), one would expect a lower D/M and D/G with the MW, LMC or SMC calibrations than with the DC16 calibrations. This is explored in Section 5.2.

## 5. APPLICATION TO THE ESTIMATION OF DEPLETIONS, D/M, AND D/G IN DLAS

In this Section, we apply the calibrations of depletions as a function of  $[\text{Zn}/\text{Fe}]$  established in the MW, LMC, and SMC to gas-phase  $[\text{Zn}/\text{Fe}]$  measurements obtained in DLAs in order to derive depletions and D/G in those systems. We choose to keep the different calibrations established in the MW, LMC, and SMC separate in order to evaluate their potential differences and the result-

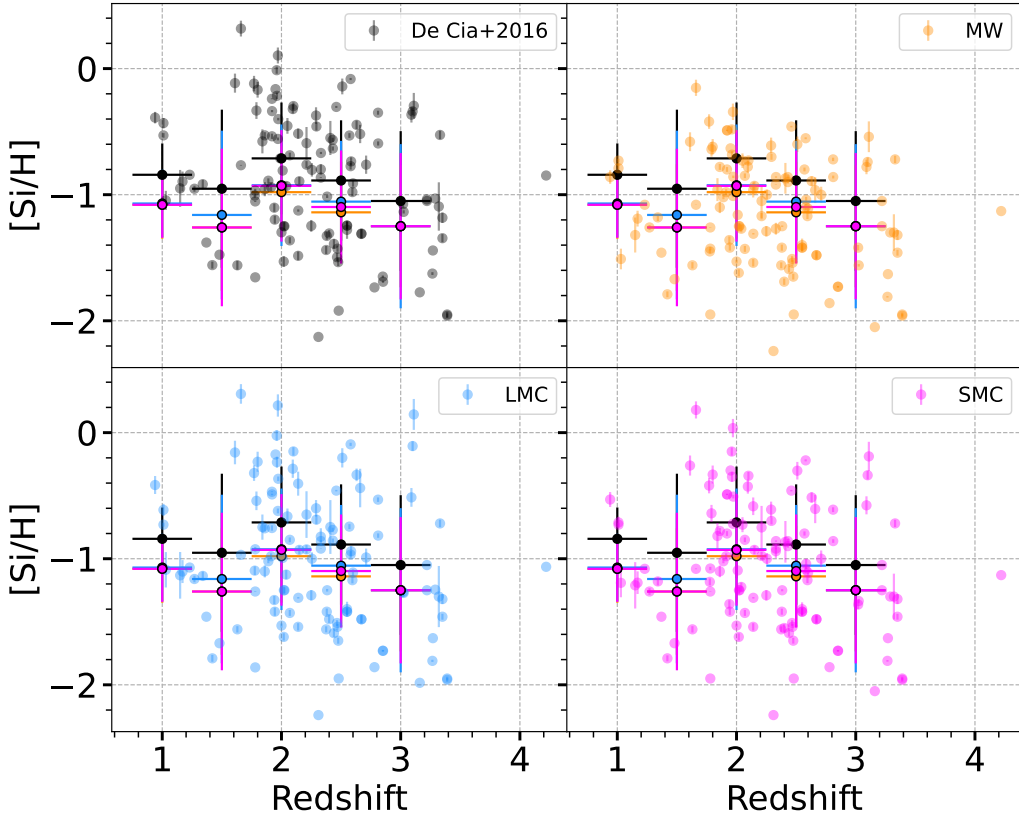


**Figure 7.** Total, depletion-corrected Si metallicities ( $[\text{Si}/\text{H}]$ ) in DLAs as a function of redshift. Depletion corrections used to estimate the total metallicities were inferred using the relation between  $[\text{Zn}/\text{Fe}]$  and depletions derived in De Cia et al. (2016) (top left), the MW (top right), the LMC (bottom left) and the SMC (bottom right). We plot the binned median for each calibration in all the panels for easy comparison (opaque circles with black outlines).

ing impact on depletion estimations in DLA systems, where abundance ratios are the only possible approach to estimate D/M and D/G. If future studies using either larger depletion samples in the MW, LMC and SMC (e.g., HST AR-16133) or depletion samples at lower metallicity (e.g., HST GO-15880) confirm that the relation between depletions of different elements, and thus the relation between abundance ratios such as  $[\text{Zn}/\text{Fe}]$  and depletions, does not strongly depend on metallicity, then it will be possible to combine those relations to derive a unique calibration of depletions as a function of abundance ratios,  $[\text{Zn}/\text{Fe}]$  in particular.

### 5.1. Depletions and total abundances in DLAs

The individual depletion estimates in DLAs obtained from each calibration (MW, LMC, SMC, DC16) are plotted in Figure 5 (points). We note that, when the depletion inferred from this approach exceeds zero (i.e., the fraction of metals in gas is  $>1$ , which is physically impossible), we set the depletion value to zero. This explains the horizontal streaks of points with zero de-

pletion in Figure 5.

As discussed in Section 4.3, for Fe and other refractory elements, the differences between the DC16 and MW/LMC/SMC calibrations of the  $[\text{Zn}/\text{Fe}]$ —depletion relation are small in the typical  $[\text{Zn}/\text{Fe}]$  range for DLAs (0—1.5). As a result, the total  $[\text{Fe}/\text{H}]$  metallicity of DLAs (corrected for depletion effects) inferred from the MW, LMC, or SMC relations between  $[\text{Zn}/\text{Fe}]$  and depletions very similar to those inferred in DC16, as shown in Figure 6.

As explained in Section 4.3, differences between the DC16 and MW/LMC/SMC calibrations are larger for volatile elements (C, O, Mg, S, Zn, Si to some extent), particularly in the low  $[\text{Zn}/\text{Fe}]$  range of the DLA sample typically associated with low metallicity. For volatile elements, the DLA depletions inferred from the MW, LMC, and SMC calibrations are generally less negative than those derived using the prescription by DC16. One would expect a lower D/M from the MW, LMC, and SMC calibrations than for the DC16 calibrations as a result, and this is examined in the next Sections (5.3 and 5.2).

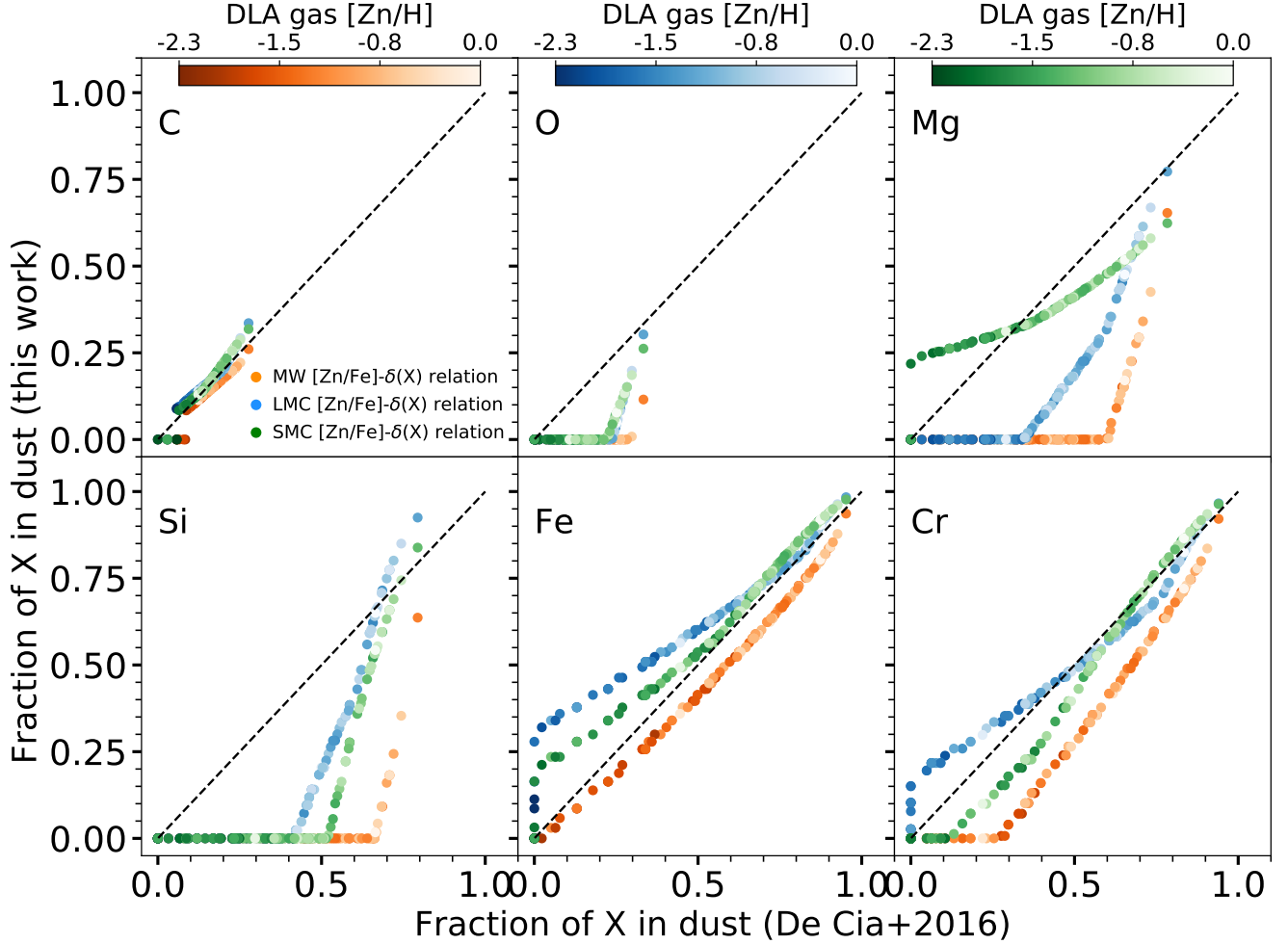


**Figure 8.** Comparison of the fraction of each element (C, O, Mg, Si, Fe, Cr) in the dust phase in DLAs obtained from the De Cia et al. (2016) calibration of the  $[\text{Zn}/\text{Fe}]$ – $\delta(X)$  relation (x-axis) and the local calibrations measured in the MW (orange color scale), LMC (blue color scale), and SMC (green color scale) shown in the y-axis. Each point corresponds to a DLA system and is color-coded by its (total) metallicity  $[\text{Fe}/\text{H}]$ , as indicated by the color bars. The black dashed line indicates a 1:1 correspondence.

As a consequence of these differences, the total metallicity difference between the MW/LMC/SMC calibrations and the DC16 calibration for volatile elements can reach 0.5 dex in some cases, particularly Si and Mg in the MW (see Figure 6). These differences, while noticeable, do not qualitatively affect the variations of the total metallicity in DLAs as a function of redshift, as shown in Figure 7. However, the baseline level of the redshift evolution of the total abundances of volatile elements (e.g., Si, Mg) with the MW calibration is about 0.5 dex (factor 3) lower than with the DC16 calibration. With the LMC and SMC calibrations, the total abundances of volatile elements are about a factor 2 lower than with the DC16 calibration. These systematic differences are significantly higher than the statistical uncertainties on gas-phase abundance measurements. We note that redshifts beyond 4 place the Zn II lines in the NIR

where they are more difficult to measure, especially given the very low metallicity of high-redshift systems. As a result, samples of DLAs with Zn abundances can only track the cosmic enrichment of the universe out to  $z \sim 3.5$ .

## 5.2. $D/G$ in DLAs

The fraction of C, O, Mg, Si, Fe, Cr in dust ( $1-10^{\delta(X)}$ ) in DLAs is derived from the depletions computed from the DC16, MW, LMC, and SMC  $[\text{Zn}/\text{Fe}]$ – $\delta(X)$  calibrations. The fractions of those elements in dust are shown in Figure 8. As expected from the generally lower depletion levels obtained from the local MW, LMC and SMC calibrations (Section 4.3, Figure 5), the fraction of Si, Mg, and O in dust are lower with the local calibrations compared to the DC16 prescription. The two

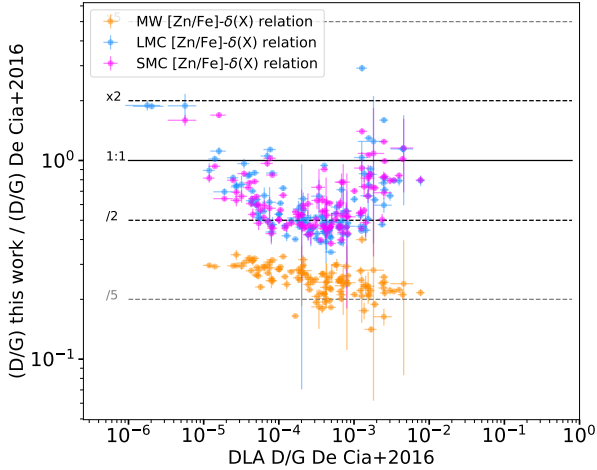


**Figure 9.** Comparison of the D/G in DLAs inferred using the relation between  $[\text{Zn}/\text{Fe}]$  and depletions derived in De Cia et al. (2016) and from the  $[\text{Zn}/\text{Fe}]$ —depletion relation observed in the MW, LMC, or SMC. The solid black line indicates a 1:1 correspondence, while the dashed lines indicate factors of 2 (black) and 5 (gray) differences.

exceptions are C (the dust fractions are similar with all calibrations) and Fe (differences are small, but the LMC and SMC calibrations lead to slightly higher dust fractions than DC16). At low metallicity, the dust fraction of Mg obtained from the SMC calibration and the dust fraction of Cr obtained from the LMC calibration are a bit higher than the dust fraction obtained from DC16.

With the fraction of each element in dust in the DLA samples, we can now compute the D/G in those systems as described in Section 2.4, for each of the  $[\text{Zn}/\text{Fe}]$ —depletion calibrations (DC16, MW, LMC, SMC). The computation of D/G in DLAs based on the DC16 calibration is identical to the one shown in Péroux & Howk (2020). As expected from the lower fractions of metals in dust obtained with the MW/LMC/SMC calibrations of the  $[\text{Zn}/\text{Fe}]$ —depletion relation compared to the DC16 relation, the D/G obtained in DLAs with the MW/LMC/SMC calibrations is lower than the one obtained using the DC16 calibration (Figure 9). The difference amounts to a factor 2 for the LMC and SMC calibrations, and a factor 5 for the MW calibration.

The relation between metallicity and D/G in DLAs, where D/G is derived from the MW/LMC/SMC calibrations of the  $[\text{Zn}/\text{Fe}]$ —depletion relation are shown in Figures 12 (MW), 13 (LMC), and 14 (SMC). Using the MW, LMC, or SMC relations between depletions and  $[\text{Zn}/\text{Fe}]$ , the metallicity—D/G trend in DLAs lies lower than with the DC16 calibration (Figure 1). This is expected since overall, the D/G derived from the MW, LMC, and SMC calibrations is a factor 2-5 lower than the D/G derived from the DC16 calibration.

This exemplifies the sensitivity of D/G estimations based on  $[\text{Zn}/\text{Fe}]$  to small “tweaks” in the calibrations of depletions vs  $[\text{Zn}/\text{Fe}]$ . The four calibrations examined here (DC16, MW, LMC, SMC) shown in Figure 5 are not dramatically different qualitatively speaking. They differ essentially by the choice of functional form as depletions approach zero level. However, due to the steepness of the slopes of those calibrations, such innocuous choices in formalism can result in substantially large results in D/G estimates.

Unfortunately, while different depletion calibrations (DC16, MW, LMC, SMC) can shift the trend of D/G vs.  $Z$  up and down, they cannot resolve the tension between D/G measured from FIR in nearby galaxies and D/G measured from  $[\text{Zn}/\text{Fe}]$  in DLAs. Indeed, the DLA metallicity—D/G relation derived from the MW/LMC/SMC depletion calibrations still appears much more linear than the trend predicted by chemical evolution models (Feldmann 2015) and observed in the FIR below  $\sim 10\%$  solar metallicity. This suggests that either the FIR-based measurements at low metallicity suffer from large systematics due to lack of robust constraint on the FIR opacity and/or the calibrations of the  $[\text{Zn}/\text{Fe}]$ —depletion relation derived at SMC metallicity and higher are not applicable to lower metallicity systems ( $< 20\%$  solar). In particular, an  $\alpha$ -enhancement of Zn in some DLAs (e.g., Fig. 9 in Rafelski et al. 2012) would cause  $[\text{Zn}/\text{Fe}]$  to be higher than predicted from the level of dust depletion in these systems. In turn, this would result in an overestimation of the level of depletion and subsequently of D/G in DLA systems (Figure 5), particularly at low metallicity where the  $\alpha$ -enhancement of Zn should be the largest (da Silva et al. 2018). Depletion measurements for a complete set of elements (C, O, Mg, Si, S, Zn, Fe) at metallicities lower than 20% solar and observational calibrations of the FIR opacity of dust will therefore be necessary to resolve this discrepancy. An additional possible source of discrepancy is the presence of an unaccounted for metal-poor HI in around low metallicity dwarf galaxies, which would bias the measurement of D/G based on FIR + 21 cm + CO 1-0 low.

In particular, the contribution of C and O to the dust budget has not been measured outside the MW. In this analysis, we used the depletions of Fe measured in the MW, LMC, SMC, or DLAs, combined with the MW relation between the depletions of Fe and that of C and O in order to estimate the depletions of C and O in the Magellanic Clouds and DLA systems. While the relatively large statistical uncertainty on this estimation is propagated in our analysis, we cannot account for the large systematic uncertainty incurred by the lack of

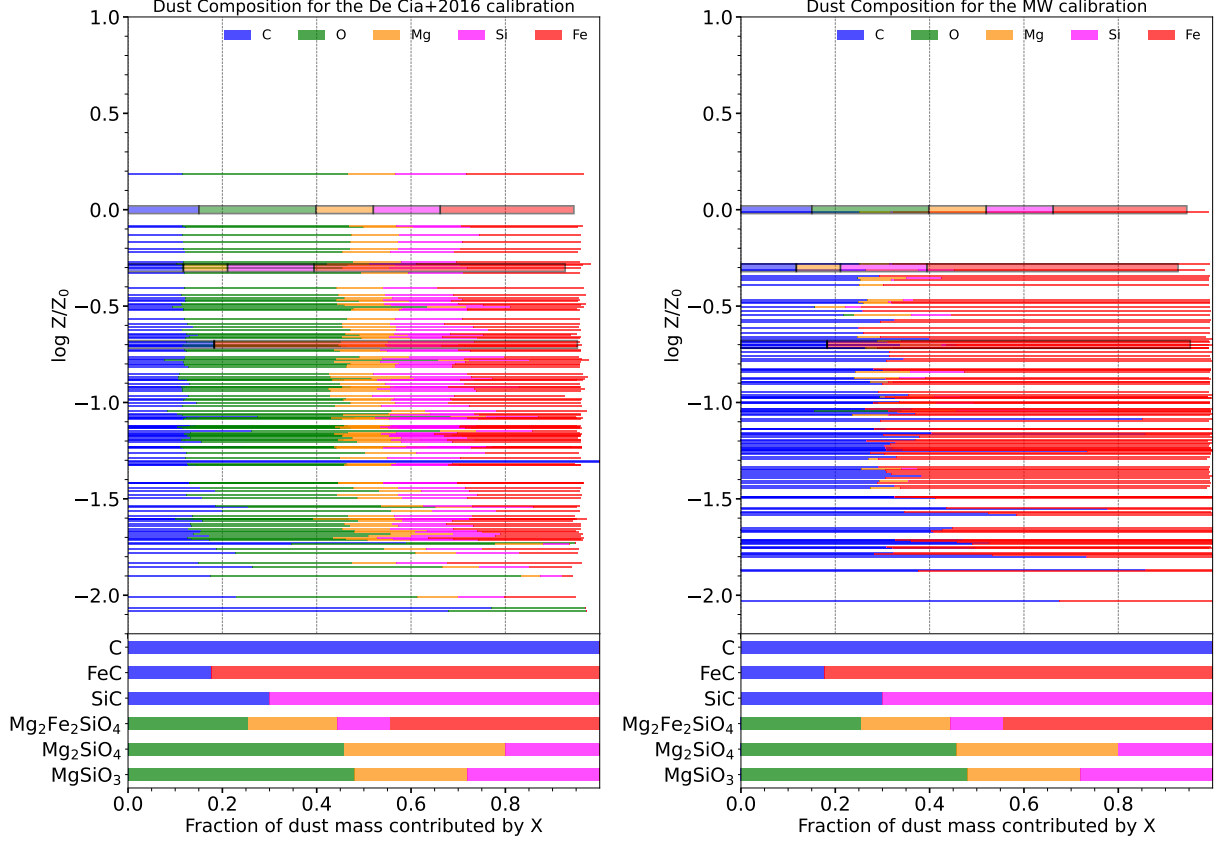


**Figure 10.** ((Top) Dust composition (i.e., fraction of the dust mass contributed by each element C, O, Mg, Si, Fe) as a function of metallicity in DLAs, the MW, LMC, and SMC. The MW, LMC, and SMC are indicated by black outlines in the bar plots. (Bottom) Mass fraction of C, O, Mg, Si, Fe for known dust types: FeC (iron carbide), SiC (silicon carbide), and silicates (olivine ( $\text{Mg}_2\text{Fe}_2\text{SiO}_4$ ), forsterite ( $\text{Mg}_2\text{SiO}_4$ ), enstatite ( $\text{MgSiO}_3$ )). With the De Cia et al. (2016) calibration, the dust composition in DLAs is consistent with a mixture of carbonaceous and silicate grains. With the MW calibration, the dust composition in DLAs is inferred to be dominated by carbon and iron (iron carbide). Dust in the MW, LMC, and SMC is consistent with a mix of silicates and carbonaceous grains.

observational constraints on C and O depletions at low metallicity, and in particular how C and O depletions relate to Fe depletions. If the relation between Fe, C and O changes in a metallicity dependent way, the shape of the trend of  $D/G$  vs  $Z$  could be significantly impacted. Unfortunately, spectroscopic abundance measurements of C and O outside the MW are beyond the reach of HST, and will have to wait until the next UV flagship mission.

### 5.3. Dust composition in DLAs

The differences in  $D/G$  are associated with differences in the dust composition. The fraction of the dust mass contributed by each element  $X$ ,  $D_X$ , is given by:

$$D_X = \frac{(1 - 10^{\delta(X)}) \left( \frac{N(X)}{N_{\text{H}}} \right)_{\text{tot}} W(X)}{1.36(D/G)} \quad (8)$$

where  $\delta(X)$  are the depletions, and  $(N(X)/N_{\text{H}})_{\text{tot}}$  and  $W(X)$  are the same terms as in Equation 5 (the total abundance and atomic weight of  $X$ ).  $D_X$  is shown in Figures 10 (DC16 and MW calibrations) and 11 (LMC and SMC calibrations). For the MW, LMC, and SMC,  $D_X$  is computed for  $\log N(\text{H}) = 20.5 \text{ cm}^{-2}$ , which is the median value for DLAs with metallicities  $> 20\%$  solar. This allows for a fair comparison of the dust composition between local galaxies and DLAs. For the DLAs, we take the same approach to compute  $D_X$  as to compute  $D/G$ , i.e., the depletions are obtained from the MW, LMC, SMC, and DC16 calibrations of depletions as a function of  $[\text{Zn}/\text{Fe}]$ . The resulting dust composition obtained from each calibration is shown in each panel of Figures 10 and 11. The bottom panels of Figures 10 and 11 also show the fraction of the dust mass contributed by C, O, Mg, Si, and Fe in known condensates such as graphite, olivine, enstatite, or iron carbide. No single

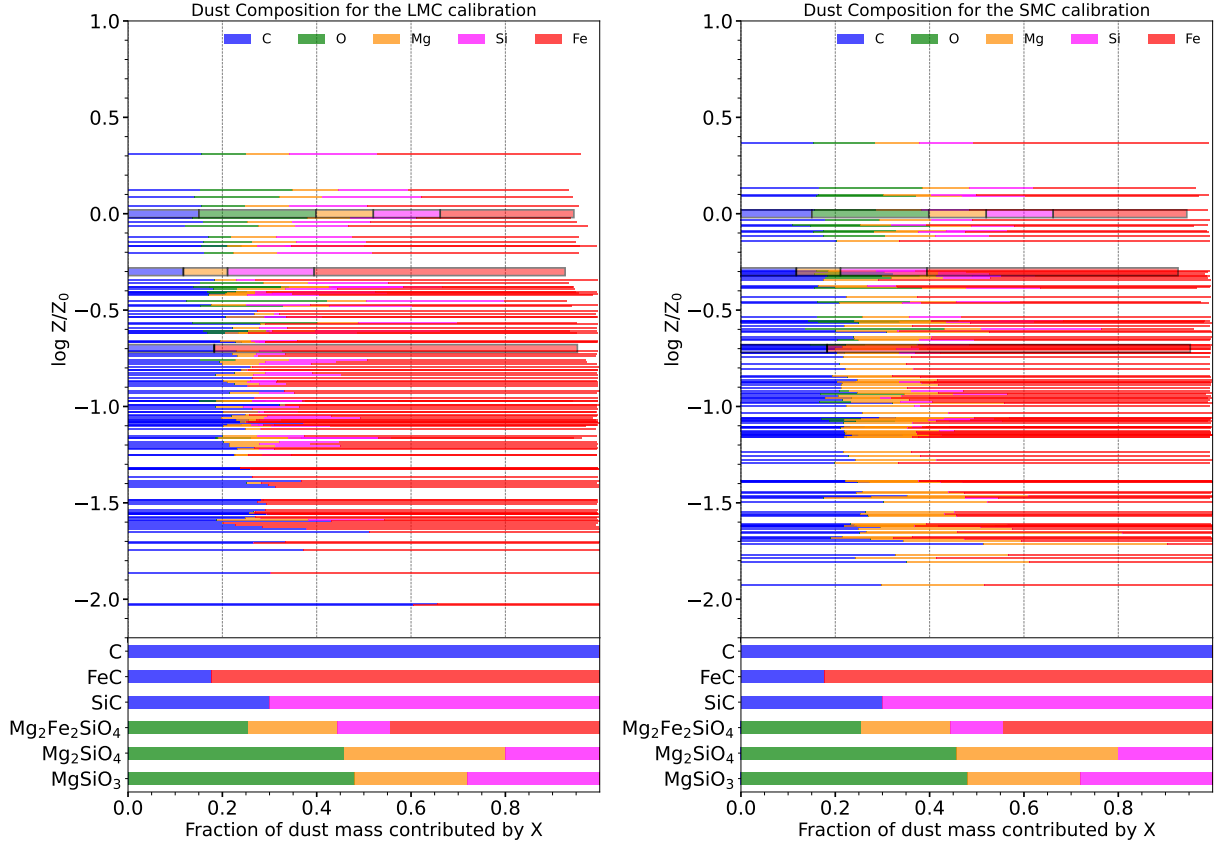


**Figure 11.** Same as Figure 10, but with the LMC and SMC calibrations of depletions applied to DLAs.

condensate matches the observed composition of dust in DLAs, indicating a mix of different dust types is present in those galaxies.

Qualitatively, the dust composition obtained in DLAs from the DC16 calibration of the  $[\text{Zn}/\text{Fe}] - \delta(X)$  relation is different from the dust composition obtained from the local calibrations (MW, LMC, SMC). With the DC16 calibration, the dust mass in DLAs is dominated by O, followed by Fe, Si, C, and Mg. This could indicate that the dust mass is predominantly composed of silicates, with a small fraction of carbonaceous grains. With the local (MW/LMC/SMC) calibrations of depletions vs  $[\text{Zn}/\text{Fe}]$ , the dust mass in DLAs is dominated by Fe (at a significantly higher fraction), followed by C. This could be consistent with a dust composition dominated by carbonaceous grains, as well as material such as iron carbide (FeC), found in pre-solar meteorites. Other elements such as O, Si, and Mg, which compose silicate grains, contribute to the dust mass at a substantially lower level, particularly at metallicities  $< 20\%$  solar.

The exception is the SMC calibration of  $[\text{Zn}/\text{Fe}] - \delta(\text{Mg})$ , which remains roughly above 10% at all metallicities. However, the  $A_{\text{Mg}}$  and  $B_{\text{Mg}}$  coefficients in the

SMC are quite uncertain (see Figures 3 and 4 of [Jenkins & Wallerstein 2017](#)), and so is the contribution of Mg to the dust mass as a result. Furthermore, the mass fraction of Mg obtained with the SMC calibration is not consistent with the stoichiometry of any known condensates (examples are shown in the bottom panels of Figures 10 and 11) pointing to possible issues with the calibration of Mg depletions in the SMC. We also note that caveat that the composition of dust in the LMC and SMC shown in Figures 10 and 11 relies on the MW relation between depletions of C, O and Fe, which could be truly different in those low metallicity environments..

The reduced fraction of silicates based on O, Mg, Si at low metallicity would be consistent with the dust properties observed in the LMC and SMC using the FIR ([Chastenot et al. 2017](#)) and UV depletions ([Roman-Duval et al. 2022](#)), where carbon dust is observed to dominate. A more detailed analysis such as the one presented in [Mattsson et al. \(2019\)](#) will be required to quantitatively constrain the dust composition in DLAs from the dust mass fractions of each element.

We make a final note that the total carbon abundance assumed in the MW to derive depletions impacts the

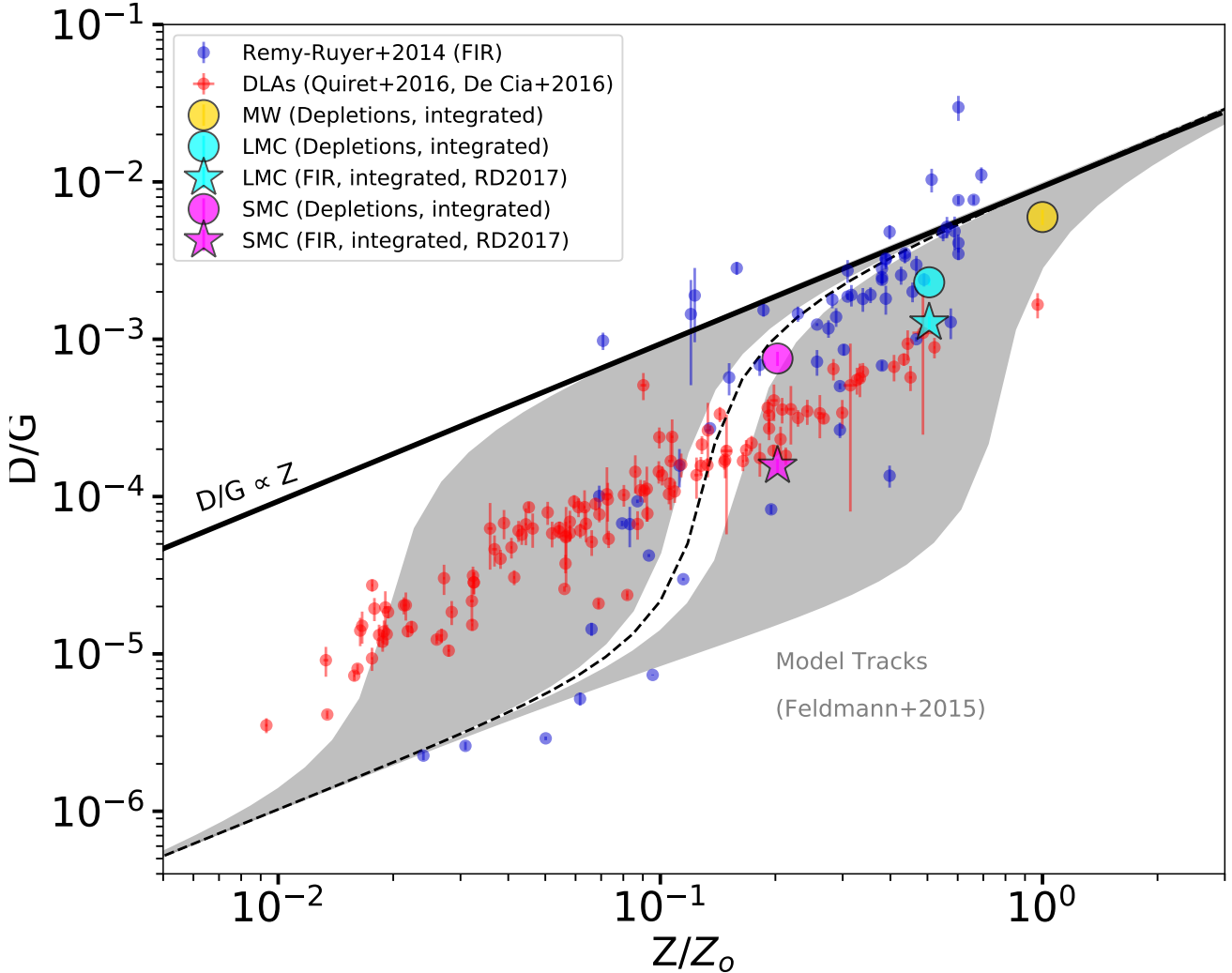


**Figure 12.** Same as Figure 1, but with the  $D/G$  in DLAs estimated using the MW relation between  $[Zn/Fe]$  and depletions.

dust composition estimated in the MW, LMC, SMC, and DLAs. In this paper as in Paper III, we assume the same carbon abundance as in the original study of MW depletions (Jenkins 2009), who in turn assume C abundances from Lodders (2003). If, instead, we assume the carbon abundance corresponding to the solar + GCE model (matching our assumed O abundance for the MW) in Table 1 of Hensley & Draine (2021), or 331 ppm, the fraction of the dust mass contributed by carbon increases by 50%.

## 6. CONCLUSION

In this paper, we compare the relations between  $[Zn/Fe]$  and other abundance ratios, which carry the imprint of depletion effects, in the neutral gas of the MW, LMC, SMC, and DLAs. We find few minor differences between these systems, albeit with a large scatter, indicating that the gas-phase  $[Zn/Fe]$  abundance ratio (and

more generally abundance ratios of volatile to refractory elements) should be good tracers of depletions in DLAs, where stellar abundances, used as proxies for total (gas + dust) ISM abundances cannot be measured (unlike the MW, LMC, or SMC).

We derive calibrations of the relation between  $[Zn/Fe]$  and interstellar depletions based on those samples of gas-phase abundances and depletions obtained in the MW, LMC and SMC, and compare those calibrations to that of De Cia et al. (2016) derived from abundance ratios in DLAs and Zn abundance measurements in the MW. We find subtle differences between those calibrations, particularly for volatile elements (Mg, Si, S), which more closely track the assumed functional form for depletions of Zn.

We apply those calibrations to samples of DLAs from the literature in order to estimate depletions,  $D/G$  and

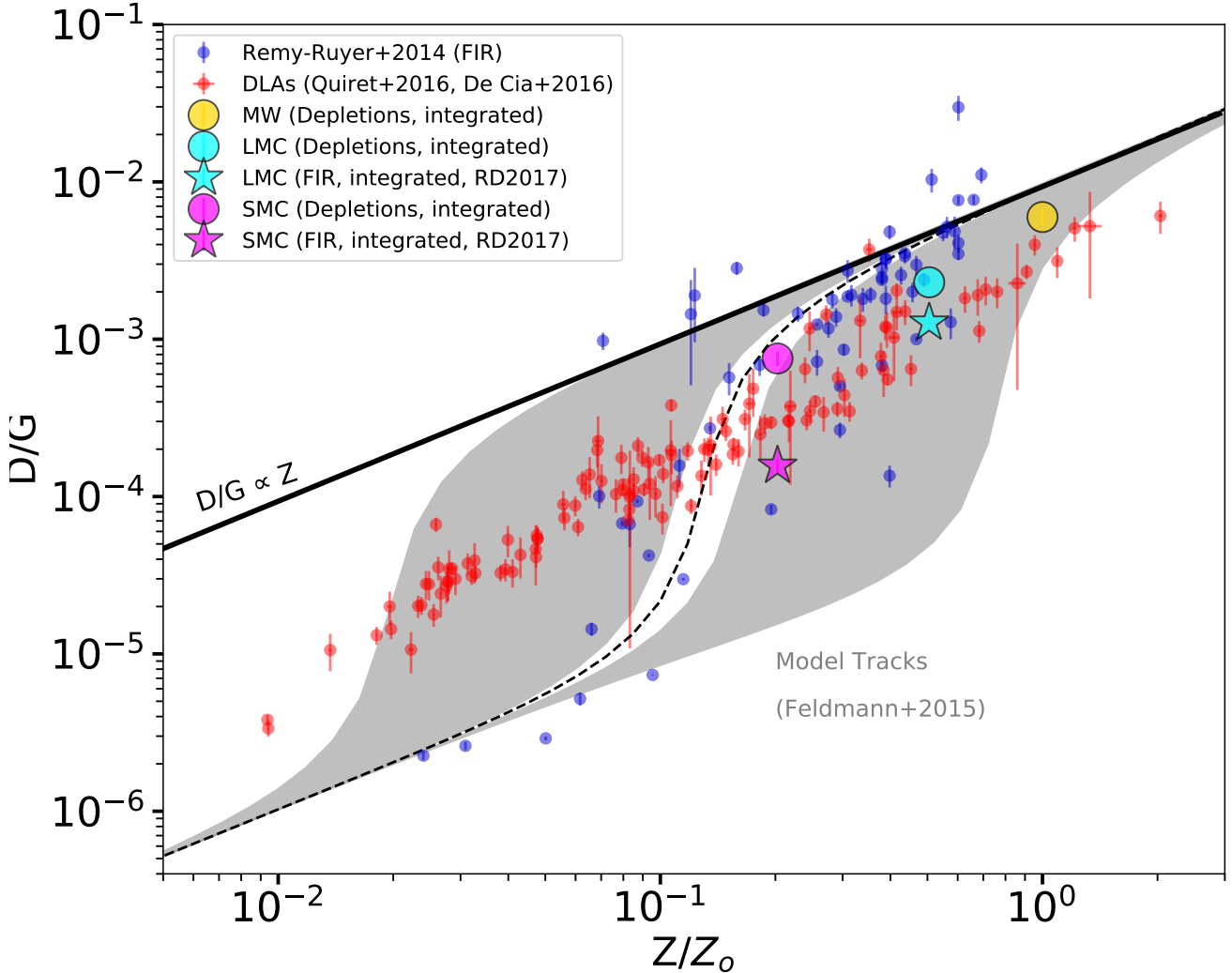


**Figure 13.** Same as Figure 1, but with the  $D/G$  in DLAs estimated using the LMC relation between  $[Zn/Fe]$  and depletions.

the dust composition in those distant systems that are key to tracking the chemical enrichment of the universe. We compare the dust abundance and composition resulting from each calibration (De Cia et al. (2016), MW, LMC, SMC), and investigate whether the subtle differences in those calibrations can explain the tension between the trend of  $D/G$  vs metallicity observed in nearby galaxies using FIR and that observed in DLAs using  $[Zn/Fe]$  to estimate  $D/G$ .

With the depletion calibrations established in the MW, LMC, and SMC, we find that the abundance of dust in DLAs is lower than with the calibration of depletions vs.  $[Zn/Fe]$  presented in DC16, on average by a factor 2 for the LMC/SMC calibrations, and a factor 5 for the MW calibration. Still, the behavior of the relation between metallicity and  $D/G$  in DLAs with all depletion calibrations (DC16, MW, LMC and SMC) ap-

pears only slightly sub-linear with metallicity, contrary to what is observed in nearby galaxies using FIR, 21 cm, and CO (1-0) emission to estimate the  $D/G$  and predicted by chemical evolution models (Feldmann 2015). Thus, the new depletion calibrations presented in this work do not resolve the tension between those two types and samples of dust abundance measurements.

Possible culprits for this tension include the poorly constrained, but varying, FIR opacity of dust; the lack of constraints on depletions of C and O outside the MW and in particular at low metallicity; the inapplicability of the calibrations between  $[Zn/Fe]$  and depletions established in the MW, LMC, or SMC to lower metallicity DLA systems; and the possible nucleosynthetic enhancement of Zn at low metallicity. Observational constraints on the FIR opacity of dust outside the MW, and samples of neutral gas abundances and depletions at metallic-



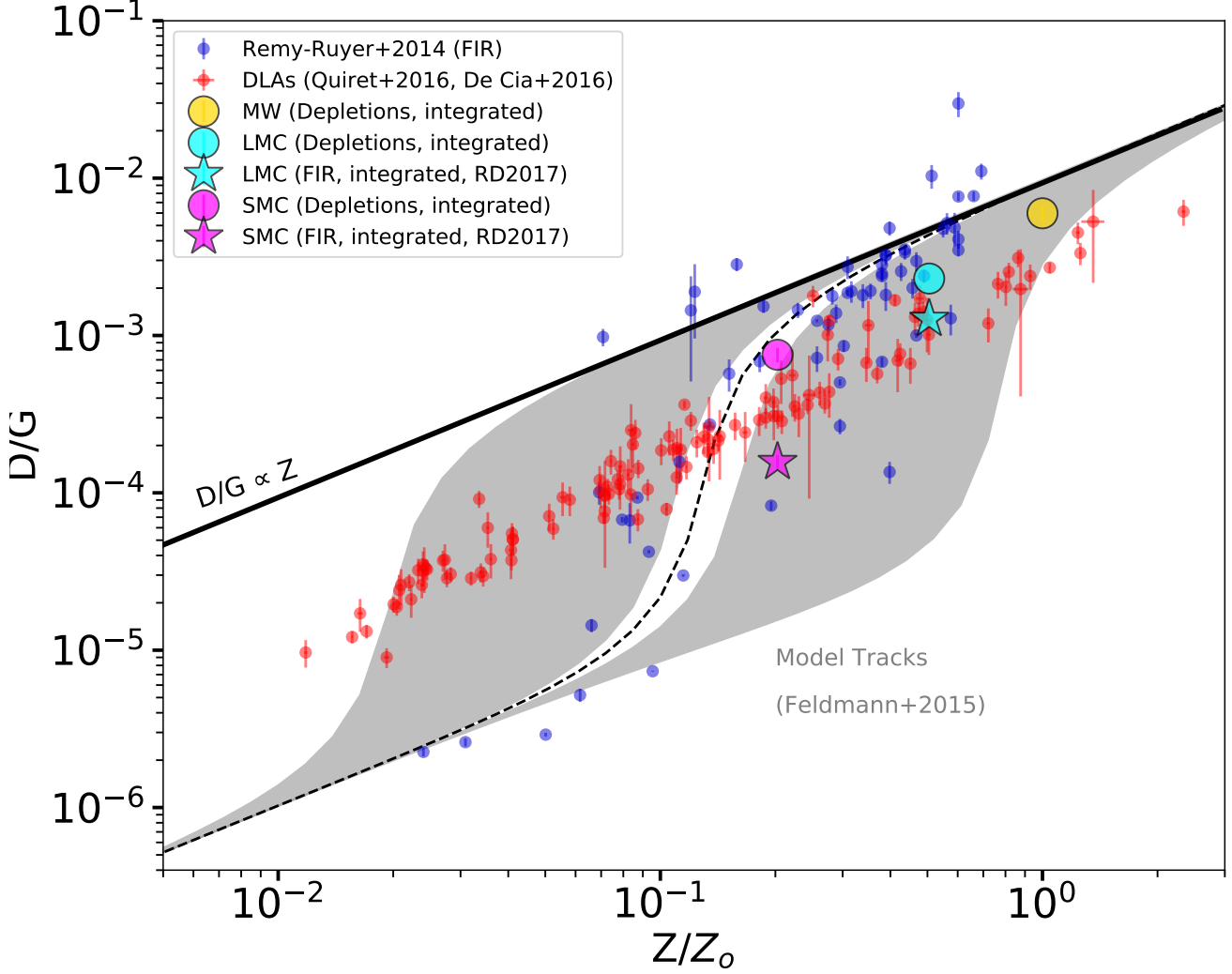


**Figure 14.** Same as Figure 1, but with the  $D/G$  in DLAs estimated using the SMC relation between  $[Zn/Fe]$  and depletions.

ties lower than 20% solar are necessary to resolve this tension.

The lower dust abundance in DLAs estimated from the MW/LMC/SMC depletion calibrations does not impact the redshift evolution of the (total) abundance of Fe in DLAs, but does lower the abundance of Si and Mg by 0.5 dex for the MW calibration (though the shape of the trend remains unchanged).

The depletion calibrations derived in this work based on MW, LMC and SMC abundance measurements predict different dust compositions in DLAs compared to the DC16 calibration. With the latter, the dust mass budget is predicted to be dominated by O, followed by Fe, Si, C, and Mg (all above 10% of the dust mass), consistent with a high abundance of silicates. Conversely with the MW/LMC/SMC calibrations, the dust mass is dominated by Fe ( $\approx 70\text{-}80\%$ ) followed by C ( $\approx 20\text{-}30\%$ ).

The fraction of the dust mass contributed by O, Mg, Si (i.e., silicates) is much smaller ( $\ll 10\%$ ). This is consistent with results obtained from the FIR in the low-metallicity LMC and SMC, showing that the fraction of silicates relative to carbon is small (Chasten et al. 2017).

For all calibrations, we caution that the dust abundance ( $D/G$ ) and composition in DLAs presented in this work rely on the same assumption to account for C and O in the dust mass budget: that the relation between the depletions of Fe and the depletions of C or O follow the relation measured in the MW. This limitation is imposed by the inability to measure the weak C and O lines outside the MW.

We thank the referee for an insightful, thorough, and constructive report. Edward B. Jenkins, Benjamin Williams, Karl Gordon, Karin Sandstrom, and Petia Yanchulova Merica-Jones acknowledge support from grant HST-GO-14675. This work is based on observations with the NASA/ESA Hubble Space Telescope obtained at the Space Telescope Science Institute, which is operated by the Associations of Universities for Research in Astronomy, Incorporated, under NASA contract NAS5-26555. These observations are associated with program 14675. Support for Program number 14675 was provided by NASA through a grant from the Space Telescope Science Institute, which is operated by the Association of Universities for Research in Astronomy, Incorporated, under NASA contract NAS5-26555.

## REFERENCES

- 2004, Origin and Evolution of the Elements  
 Asano, R. S., Takeuchi, T. T., Hirashita, H., & Inoue, A. K. 2013, *Earth, Planets, and Space*, 65, 213, doi: [10.5047/eps.2012.04.014](https://doi.org/10.5047/eps.2012.04.014)
- Asplund, M., Grevesse, N., Sauval, A. J., & Scott, P. 2009, *ARA&A*, 47, 481, doi: [10.1146/annurev.astro.46.060407.145222](https://doi.org/10.1146/annurev.astro.46.060407.145222)
- Bigieli, F., Leroy, A., Walter, F., et al. 2008, *AJ*, 136, 2846, doi: [10.1088/0004-6256/136/6/2846](https://doi.org/10.1088/0004-6256/136/6/2846)
- Bolatto, A. D., Wolfire, M., & Leroy, A. K. 2013, *ARA&A*, 51, 207, doi: [10.1146/annurev-astro-082812-140944](https://doi.org/10.1146/annurev-astro-082812-140944)
- Chastenet, J., Bot, C., Gordon, K. D., et al. 2017, *A&A*, 601, A55, doi: [10.1051/0004-6361/201629133](https://doi.org/10.1051/0004-6361/201629133)
- Chastenet, J., Sandstrom, K., Chiang, I.-D., et al. 2019, *ApJ*, 876, 62, doi: [10.3847/1538-4357/ab16cf](https://doi.org/10.3847/1538-4357/ab16cf)
- Chiang, I.-D., Sandstrom, K. M., Chastenet, J., et al. 2021, *ApJ*, 907, 29, doi: [10.3847/1538-4357/abceb6](https://doi.org/10.3847/1538-4357/abceb6)
- Clark, C. J. R., De Vis, P., Baes, M., et al. 2019, *MNRAS*, 489, 5256, doi: [10.1093/mnras/stz2257](https://doi.org/10.1093/mnras/stz2257)
- Cooke, R., Pettini, M., Steidel, C. C., Rudie, G. C., & Nissen, P. E. 2011, *MNRAS*, 417, 1534, doi: [10.1111/j.1365-2966.2011.19365.x](https://doi.org/10.1111/j.1365-2966.2011.19365.x)
- da Silveira, C. R., Barbuy, B., Friaça, A. C. S., et al. 2018, *A&A*, 614, A149, doi: [10.1051/0004-6361/201730562](https://doi.org/10.1051/0004-6361/201730562)
- De Cia, A. 2018, *A&A*, 613, L2, doi: [10.1051/0004-6361/201833034](https://doi.org/10.1051/0004-6361/201833034)
- De Cia, A., Ledoux, C., Mattsson, L., et al. 2016, *A&A*, 596, A97, doi: [10.1051/0004-6361/201527895](https://doi.org/10.1051/0004-6361/201527895)
- De Cia, A., Ledoux, C., Petitjean, P., & Savaglio, S. 2018, *A&A*, 611, A76, doi: [10.1051/0004-6361/201731970](https://doi.org/10.1051/0004-6361/201731970)
- De Cia, A., Ledoux, C., Savaglio, S., Schady, P., & Vreeswijk, P. M. 2013, *A&A*, 560, A88, doi: [10.1051/0004-6361/201321834](https://doi.org/10.1051/0004-6361/201321834)
- De Vis, P., Jones, A., Viaene, S., et al. 2019, *A&A*, 623, A5, doi: [10.1051/0004-6361/201834444](https://doi.org/10.1051/0004-6361/201834444)
- Delgado Mena, E., Moya, A., Adibekyan, V., et al. 2019, *A&A*, 624, A78, doi: [10.1051/0004-6361/201834783](https://doi.org/10.1051/0004-6361/201834783)
- Demyk, K., Meny, C., Leroux, H., et al. 2017, *A&A*, 606, A50, doi: [10.1051/0004-6361/201730944](https://doi.org/10.1051/0004-6361/201730944)
- Duffau, S., Caffau, E., Sbordone, L., et al. 2017, *A&A*, 604, A128, doi: [10.1051/0004-6361/201730477](https://doi.org/10.1051/0004-6361/201730477)
- Ernandes, H., Barbuy, B., Alves-Brito, A., et al. 2018, *A&A*, 616, A18, doi: [10.1051/0004-6361/201731708](https://doi.org/10.1051/0004-6361/201731708)
- Feldmann, R. 2015, *MNRAS*, 449, 3274, doi: [10.1093/mnras/stv552](https://doi.org/10.1093/mnras/stv552)
- Fumagalli, M., O’Meara, J. M., & Prochaska, J. X. 2016, *MNRAS*, 455, 4100, doi: [10.1093/mnras/stv2616](https://doi.org/10.1093/mnras/stv2616)
- Galliano, F., Galametz, M., & Jones, A. P. 2018, *ARA&A*, 56, 673, doi: [10.1146/annurev-astro-081817-051900](https://doi.org/10.1146/annurev-astro-081817-051900)
- Heintz, K. E., & Watson, D. 2020, *ApJL*, 889, L7, doi: [10.3847/2041-8213/ab6733](https://doi.org/10.3847/2041-8213/ab6733)
- Hensley, B. S., & Draine, B. T. 2021, *ApJ*, 906, 73, doi: [10.3847/1538-4357/abc8f1](https://doi.org/10.3847/1538-4357/abc8f1)
- Hill, V., Andrievsky, S., & Spite, M. 1995, *A&A*, 293, 347
- Hirashita, H. 2000, *PASJ*, 52, 585, doi: [10.1093/pasj/52.4.585](https://doi.org/10.1093/pasj/52.4.585)
- Jenkins, E. B. 2009, *ApJ*, 700, 1299, doi: [10.1088/0004-637X/700/2/1299](https://doi.org/10.1088/0004-637X/700/2/1299)
- Jenkins, E. B., & Wallerstein, G. 2017, *ApJ*, 838, 85, doi: [10.3847/1538-4357/aa64d4](https://doi.org/10.3847/1538-4357/aa64d4)

- Kisielius, R., Kulkarni, V. P., Ferland, G. J., Bogdanovich, P., & Lykins, M. L. 2014, *ApJ*, 780, 76, doi: [10.1088/0004-637X/780/1/76](https://doi.org/10.1088/0004-637X/780/1/76)
- Kisielius, R., Kulkarni, V. P., Ferland, G. J., et al. 2015, *ApJ*, 804, 76, doi: [10.1088/0004-637X/804/1/76](https://doi.org/10.1088/0004-637X/804/1/76)
- Lodders, K. 2003, *Meteoritics and Planetary Science Supplement*, 38, 5272
- . 2021, *SSRv*, 217, 44, doi: [10.1007/s11214-021-00825-8](https://doi.org/10.1007/s11214-021-00825-8)
- Mattsson, L., De Cia, A., Andersen, A. C., & Petitjean, P. 2019, *A&A*, 624, A103, doi: [10.1051/0004-6361/201731482](https://doi.org/10.1051/0004-6361/201731482)
- Morton, D. C. 2003, *ApJS*, 149, 205, doi: [10.1086/377639](https://doi.org/10.1086/377639)
- Noterdaeme, P., Ledoux, C., Petitjean, P., & Srianand, R. 2008, *A&A*, 481, 327, doi: [10.1051/0004-6361:20078780](https://doi.org/10.1051/0004-6361:20078780)
- O'Meara, J. M., Prochaska, J. X., Burles, S., et al. 2007, *ApJ*, 656, 666, doi: [10.1086/510711](https://doi.org/10.1086/510711)
- Péroux, C., & Howk, J. C. 2020, *ARA&A*, 58, 363, doi: [10.1146/annurev-astro-021820-120014](https://doi.org/10.1146/annurev-astro-021820-120014)
- Pettini, M., Zych, B. J., Steidel, C. C., & Chaffee, F. H. 2008, *MNRAS*, 385, 2011, doi: [10.1111/j.1365-2966.2008.12951.x](https://doi.org/10.1111/j.1365-2966.2008.12951.x)
- Prochaska, J. X., Herbert-Fort, S., & Wolfe, A. M. 2005, *ApJ*, 635, 123, doi: [10.1086/497287](https://doi.org/10.1086/497287)
- Quiret, S., Péroux, C., Zafar, T., et al. 2016, *MNRAS*, 458, 4074, doi: [10.1093/mnras/stw524](https://doi.org/10.1093/mnras/stw524)
- Rafelski, M., Wolfe, A. M., Prochaska, J. X., Neeleman, M., & Mendez, A. J. 2012, *ApJ*, 755, 89, doi: [10.1088/0004-637X/755/2/89](https://doi.org/10.1088/0004-637X/755/2/89)
- Rémy-Ruyer, A., Madden, S. C., Galliano, F., et al. 2014, *A&A*, 563, A31, doi: [10.1051/0004-6361/201322803](https://doi.org/10.1051/0004-6361/201322803)
- Roman-Duval, J., Bot, C., Chastenet, J., & Gordon, K. 2017, *ApJ*, 841, 72, doi: [10.3847/1538-4357/aa7067](https://doi.org/10.3847/1538-4357/aa7067)
- Roman-Duval, J., Gordon, K. D., Meixner, M., et al. 2014, *ApJ*, 797, 86, doi: [10.1088/0004-637X/797/2/86](https://doi.org/10.1088/0004-637X/797/2/86)
- Roman-Duval, J., Jenkins, E. B., Williams, B., et al. 2019, *ApJ*, 871, 151, doi: [10.3847/1538-4357/aaf8bb](https://doi.org/10.3847/1538-4357/aaf8bb)
- Roman-Duval, J., Jenkins, E. B., Tchernyshyov, K., et al. 2021, *ApJ*, 910, 95, doi: [10.3847/1538-4357/abdeb6](https://doi.org/10.3847/1538-4357/abdeb6)
- . 2022, *ApJ*, 928, 90, doi: [10.3847/1538-4357/ac5248](https://doi.org/10.3847/1538-4357/ac5248)
- Russell, S. C., & Dopita, M. A. 1992, *ApJ*, 384, 508, doi: [10.1086/170893](https://doi.org/10.1086/170893)
- Sitnova, T. M., Yakovleva, S. A., Belyaev, A. K., & Mashonkina, L. I. 2022, arXiv e-prints, arXiv:2205.05819, <https://arxiv.org/abs/2205.05819>
- Skúladóttir, Á., Tolstoy, E., Salvadori, S., Hill, V., & Pettini, M. 2017, *A&A*, 606, A71, doi: [10.1051/0004-6361/201731158](https://doi.org/10.1051/0004-6361/201731158)
- Stepnik, B., Abergel, A., Bernard, J.-P., et al. 2003, *A&A*, 398, 551, doi: [10.1051/0004-6361:20021309](https://doi.org/10.1051/0004-6361:20021309)
- Tchernyshyov, K., Meixner, M., Seale, J., et al. 2015, *ApJ*, 811, 78, doi: [10.1088/0004-637X/811/2/78](https://doi.org/10.1088/0004-637X/811/2/78)
- Waskom, M. L. 2021, *Journal of Open Source Software*, 6, 3021, doi: [10.21105/joss.03021](https://doi.org/10.21105/joss.03021)
- Welty, D. E., & Crowther, P. A. 2010, *MNRAS*, 404, 1321, doi: [10.1111/j.1365-2966.2010.16386.x](https://doi.org/10.1111/j.1365-2966.2010.16386.x)
- Ysard, N., Jones, A. P., Demyk, K., Boutéraon, T., & Koehler, M. 2018, *A&A*, 617, A124, doi: [10.1051/0004-6361/201833386](https://doi.org/10.1051/0004-6361/201833386)

## 7. APPENDIX A

In this appendix, we describe the binary fits tables included in the online materials with this paper. There are 8 binary fits tables, one for each combination of sample (De Cia et al. (2016), Quirot et al. (2016)) and calibration (DC16, MW, LMC, SMC). The binary fits table contain the gas-phase abundance measurements for each sample, the depletions estimated from  $[\text{Zn}/\text{Fe}]$  using each calibration, and the depletion-corrected total abundances. In addition, the tables also contain gas-phase and total abundances estimated from Equation 7 for elements not measured in the DLA spectra (e.g., C, O). Lastly, the D/G and D/M, computed from Equations 5 and 6 are included in the tables. Each column of the tables are described in more details in Table 6.

Column name	Unit	Description
<i>QUASAR</i>	...	Name of DLA system
<i>Z_ABS</i>	...	Redshift of DLA system
<i>LOG_NHI</i>	$\text{cm}^{-2}$	Base 10 logarithm of the H I column density
<i>ERR_LOG_NHI</i>	$\text{cm}^{-2}$	Error on the base 10 logarithm of the H I column density
<i>LIM_LOG_NHI</i>	...	'v' ('value') if H I column is not a limit, 'u' for upper limit, 'l' for lower limit
<i>gas_A_{X}</i>	...	Measured gas-phase abundance of element X ( $X = \{\text{C}, \text{O}, \text{Mg}, \text{Si}, \text{S}, \text{Fe}, \text{Zn}, \text{Cr}\}$ ) - NaN if not measured
<i>err_gas_A_{X}</i>	...	Error on the measured gas-phase abundance of element X ( $X = \{\text{C}, \text{O}, \text{Mg}, \text{Si}, \text{S}, \text{Fe}, \text{Zn}, \text{Cr}\}$ ) - NaN if not measured
<i>lim_gas_A_{X}</i>	...	Limit of measured gas-phase abundance of element X ( $X = \{\text{C}, \text{O}, \text{Mg}, \text{Si}, \text{S}, \text{Fe}, \text{Zn}, \text{Cr}\}$ ) - 'v' for detection, 'u' for upper limit, 'l' for lower limit
<i>dep_{X}</i>	...	Depletion of element X ( $X = \{\text{C}, \text{O}, \text{Mg}, \text{Si}, \text{S}, \text{Fe}, \text{Zn}, \text{Cr}\}$ ) inferred from $[\text{Zn}/\text{Fe}]$ and a calibration (DC16, MW, LMC, or SMC) - NaN if Zn or Fe not measured
<i>err_dep_{X}</i>	...	Error on the depletion of element X ( $X = \{\text{C}, \text{O}, \text{Mg}, \text{Si}, \text{S}, \text{Fe}, \text{Zn}, \text{Cr}\}$ ) - NaN if not measured
<i>tot_A_{X}</i>	...	Total (gas + dust) abundance of element X ( $X = \{\text{C}, \text{O}, \text{Mg}, \text{Si}, \text{S}, \text{Fe}, \text{Zn}, \text{Cr}\}$ ) derived from Equation 1
<i>err_tot_A_{X}</i>	...	Error on the total abundance of element X ( $X = \{\text{C}, \text{O}, \text{Mg}, \text{Si}, \text{S}, \text{Fe}, \text{Zn}, \text{Cr}\}$ )
<i>est_tot_A_{X}</i>	...	Total abundance of element X ( $X = \{\text{C}, \text{O}, \text{Mg}, \text{Si}, \text{S}, \text{Fe}, \text{Zn}, \text{Cr}\}$ ) estimated from Equation 7
<i>err_est_tot_A_{X}</i>	...	Error on the total abundance of element X ( $X = \{\text{C}, \text{O}, \text{Mg}, \text{Si}, \text{S}, \text{Fe}, \text{Zn}, \text{Cr}\}$ ) estimated from Equation 7
<i>est_gas_A_{X}</i>	...	Gas-phase abundance of element X ( $X = \{\text{C}, \text{O}, \text{Mg}, \text{Si}, \text{S}, \text{Fe}, \text{Zn}, \text{Cr}\}$ ) estimated from Equation 7 and the depletion of X
<i>err_est_gas_A_{X}</i>	...	Error on the gas-phase abundance of element X ( $X = \{\text{C}, \text{O}, \text{Mg}, \text{Si}, \text{S}, \text{Fe}, \text{Zn}, \text{Cr}\}$ ) estimated from Equation 7 and the depletion of X
<i>DTG</i>	...	Dust-to-gas ratio estimated from Equation 5, <i>tot_A_{X}</i> if not NaN or <i>est_tot_A_{X}</i> otherwise and <i>dep_{X}</i> for $X = \{\text{C}, \text{O}, \text{Mg}, \text{Si}, \text{S}, \text{Fe}, \text{Zn}, \text{Cr}\}$
<i>err_DTG</i>	...	Error on the dust-to-gas ratio estimated from Equation 5, <i>err_tot_A_{X}</i> if not NaN or <i>err_est_tot_A_{X}</i> otherwise and <i>err_dep_{X}</i> for $X = \{\text{C}, \text{O}, \text{Mg}, \text{Si}, \text{S}, \text{Fe}, \text{Zn}, \text{Cr}\}$
<i>DTM</i>	...	Dust-to-metal ratio estimated from Equation 6, <i>tot_A_{X}</i> if not NaN or <i>est_tot_A_{X}</i> otherwise and <i>dep_{X}</i> for $X = \{\text{C}, \text{O}, \text{Mg}, \text{Si}, \text{S}, \text{Fe}, \text{Zn}, \text{Cr}\}$
<i>err_DTM</i>	...	Error on the dust-to-metal ratio estimated from Equation 6, <i>err_tot_A_{X}</i> if not NaN or <i>err_est_tot_A_{X}</i> otherwise and <i>err_dep_{X}</i> for $X = \{\text{C}, \text{O}, \text{Mg}, \text{Si}, \text{S}, \text{Fe}, \text{Zn}, \text{Cr}\}$

**Table A1.** Description of online binary fits tables

## 8. APPENDIX B

In this Appendix, we evaluate the performance of the different calibrations of the  $[\text{Zn}/\text{Fe}] - \delta(X)$  relation (DC16, MW, LMC, and SMC). We proceed by applying the calibrations to the individual  $[\text{Zn}/\text{Fe}]$  measurements in each of the local galaxy samples (MW, LMC, SMC), and by comparing the resulting depletions estimated from  $[\text{Zn}/\text{Fe}]$  to the depletion measurements obtained from the ratio of gas-phase to stellar abundances.

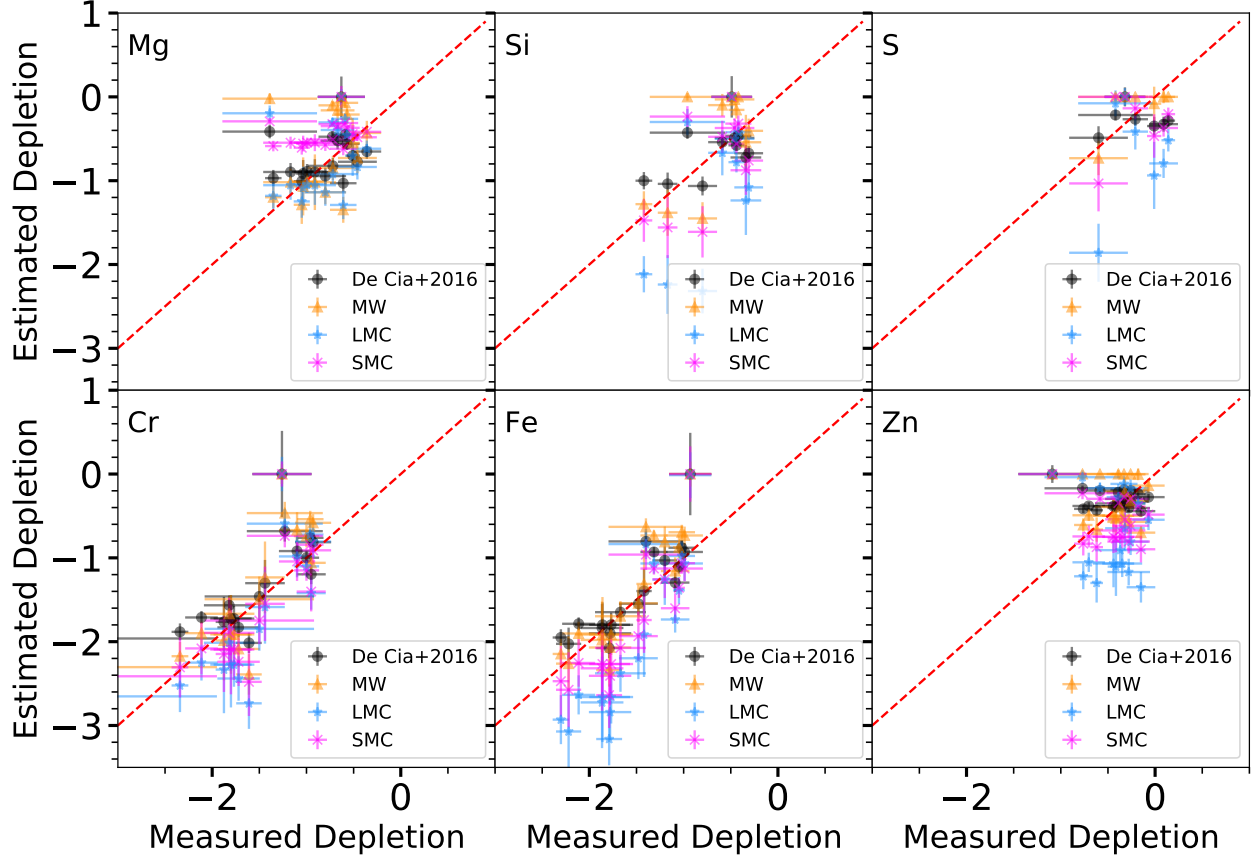


**Figure 15.** Comparison between depletions obtained from stellar and gas-phase abundances, and depletions estimated using the De Cia et al. (2016) (black), MW (orange), LMC (blue), and SMC (magenta) calibration of the  $[\text{Zn}/\text{Fe}] - \delta(X)$  relation, using the MW sample of gas-phase abundances

In Figures 15 (MW sample), 16 (LMC sample), and 17 (SMC sample), we plot the comparison between samples of depletions in each galaxy derived from gas-phase and stellar abundances and those inferred from the gas-phase  $[\text{Zn}/\text{Fe}]$  ratio and each calibration (DC16, MW, LMC, SMC). The comparison are much more favorable for refractory elements with a wide dynamic range of depletions compared to measurement uncertainties, than for volatile elements where the dynamic range in depletion is only a few times the measurement uncertainties (see also the scatter in Figure 4). In order to better discern and understand the differences in outcome between the different calibrations, we plot in Figures 15 (MW sample), 16 (LMC sample), and 17 (SMC sample) the residuals of the comparisons shown in Figures 15, 16, and 17, respectively, as a function of  $[\text{Zn}/\text{Fe}]$  for each calibration and for different elements (Mg, Si, S, Cr, Fe, Zn). In each panel corresponding to a given element, the mean and RMS residuals (corresponding to the bias and scatter) are indicated in parentheses for each of the calibrations (DC16, MW, LMC, SMC). Furthermore, the distributions of those residuals are plotted as “box plots” (Waskom 2021) in Figures 21 (MW sample), 22 (LMC sample), and 23 (SMC sample), to allow a visual comparison of the bias and accuracy of the different calibrations.

In general, the calibration of the  $[\text{Zn}/\text{Fe}] - \delta(X)$  relation performs best in the galaxy in which it was derived. The DC16 and MW calibrations result in the least bias and scatter when applied to the MW sample. Depending on the element, either the DC16 or MW calibration exhibits the least bias, but the MW calibration tends to lead to slightly higher scatter. Similarly with the LMC sample, the LMC calibration yields the least bias, closely followed by the DC16 calibration, which is slightly more biased but results in less scatter. Finally with the SMC sample, the SMC calibration results in the least bias and while the DC16 calibration results in the least scatter (but not by much).

The more important point is that the scatter in the residuals and the differences in retrieved depletions between different calibrations are much larger than the typical uncertainties on gas-phase abundance measurements. This

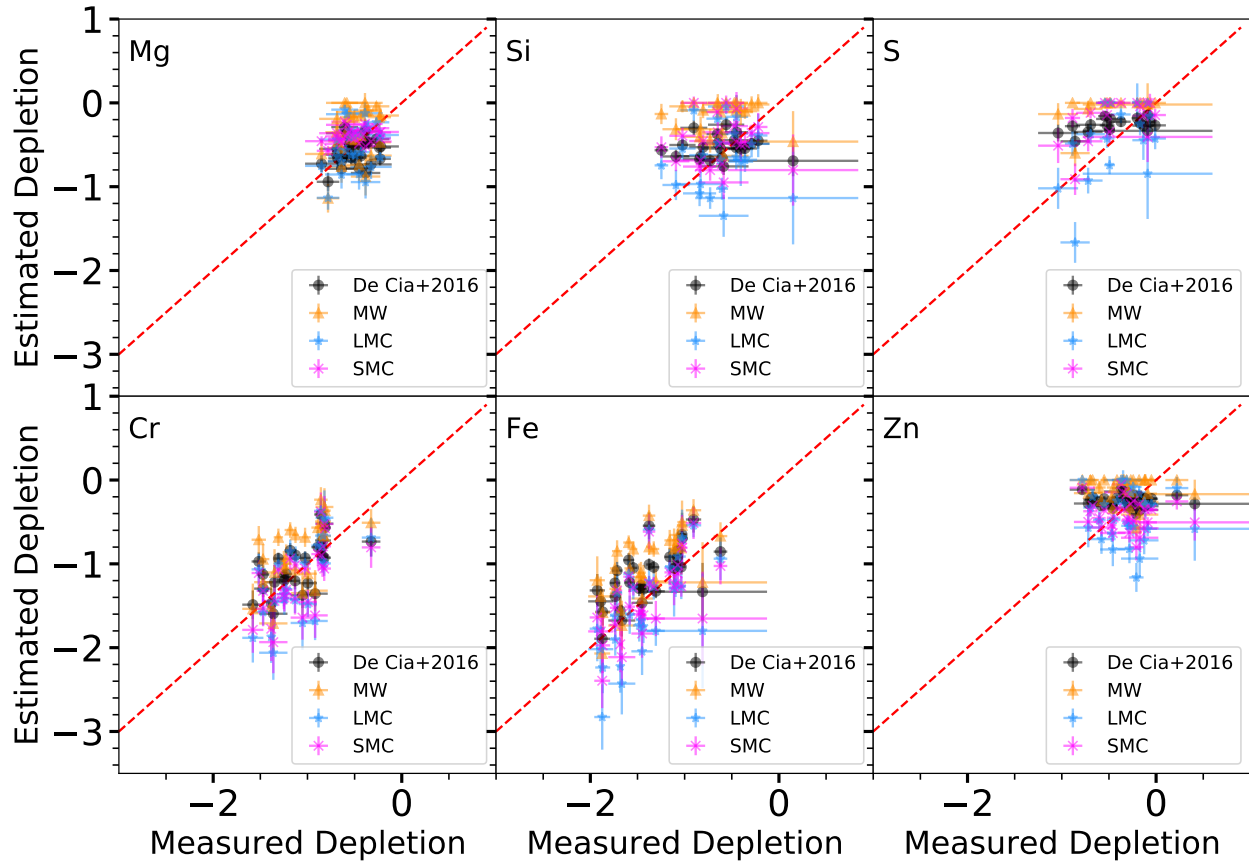


**Figure 16.** Comparison between depletions and depletions estimated using the De Cia et al. (2016) (black), MW (orange), LMC (blue), and SMC (magenta) calibration of the  $[\text{Zn}/\text{Fe}] - \delta(X)$  relation, using the LMC sample of gas-phase abundances

systematic effect should be included in the error budget for depletion and total abundance estimates in galaxies and DLAs.

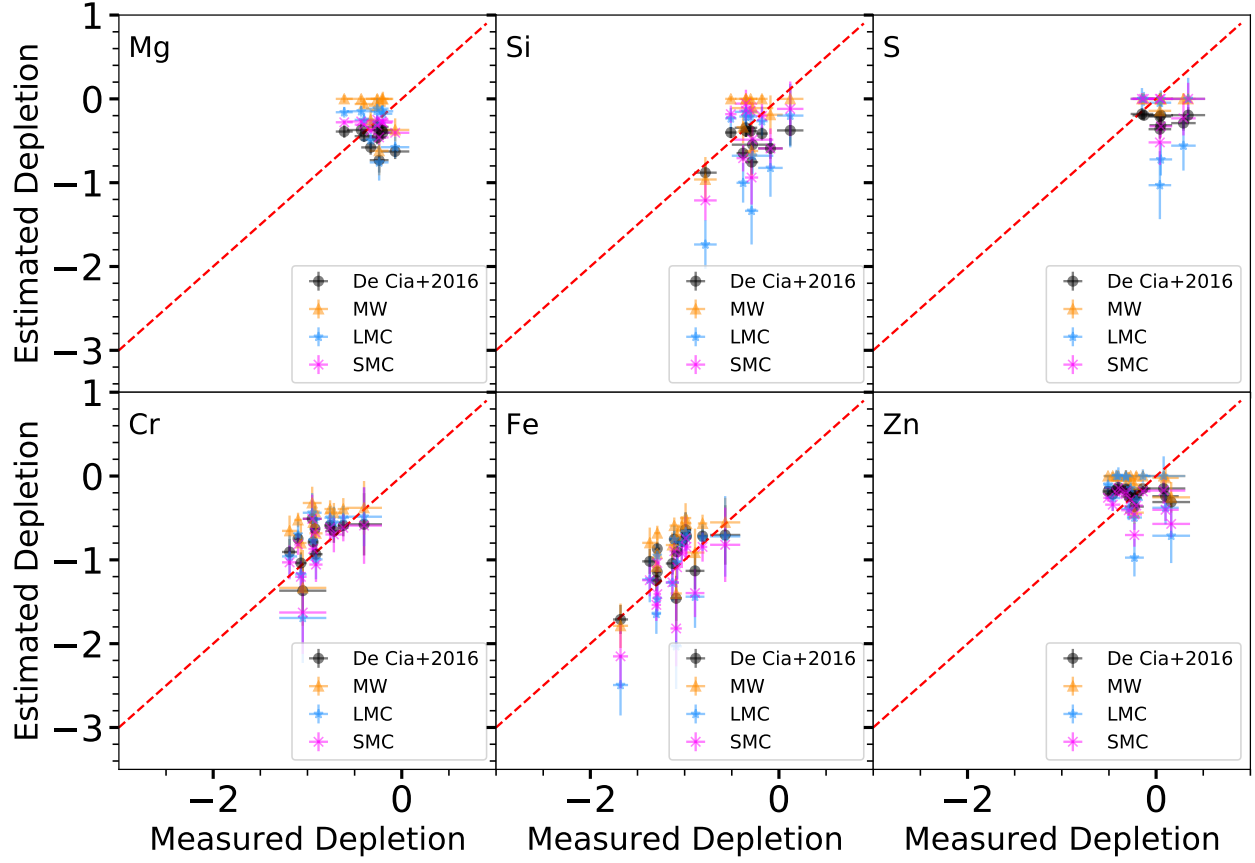


**Figure 17.** Comparison between depletions and depletions estimated using the De Cia et al. (2016) (black), MW (orange), LMC (blue), and SMC (magenta) calibration of the  $[Zn/Fe]-\delta(X)$  relation. The two residuals indicated in parentheses correspond to the mean difference and root mean square difference between the measured and estimated depletions, using the SMC sample of gas-phase abundances

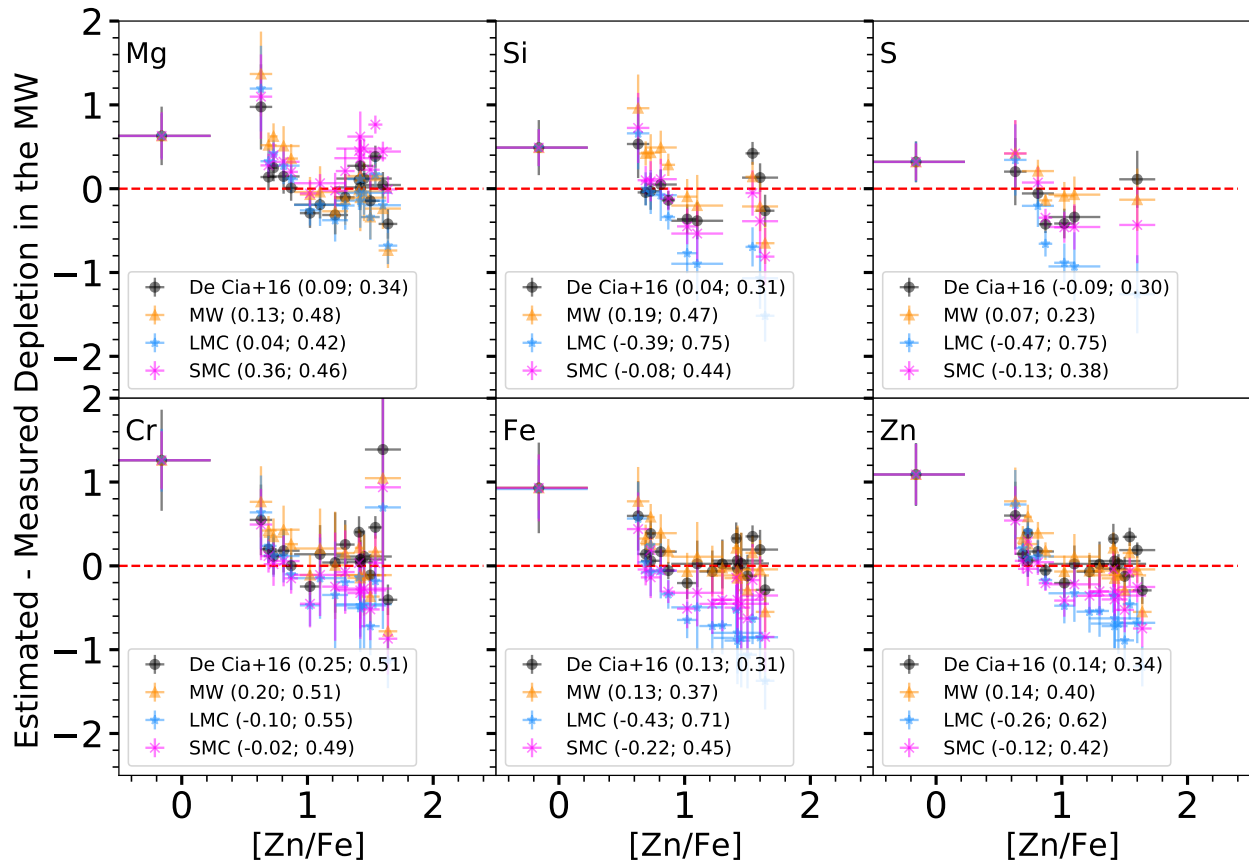


**Figure 18.** Difference in the MW sample between depletions obtained from stellar and gas-phase abundances, and depletions estimated using the De Cia et al. (2016) (black), MW (orange), LMC (blue), and SMC (magenta) calibration of the  $[Zn/Fe]$ — $\delta(X)$  relation. The two residuals indicated in parentheses correspond to the mean difference and root mean square difference between the measured and estimated depletions.



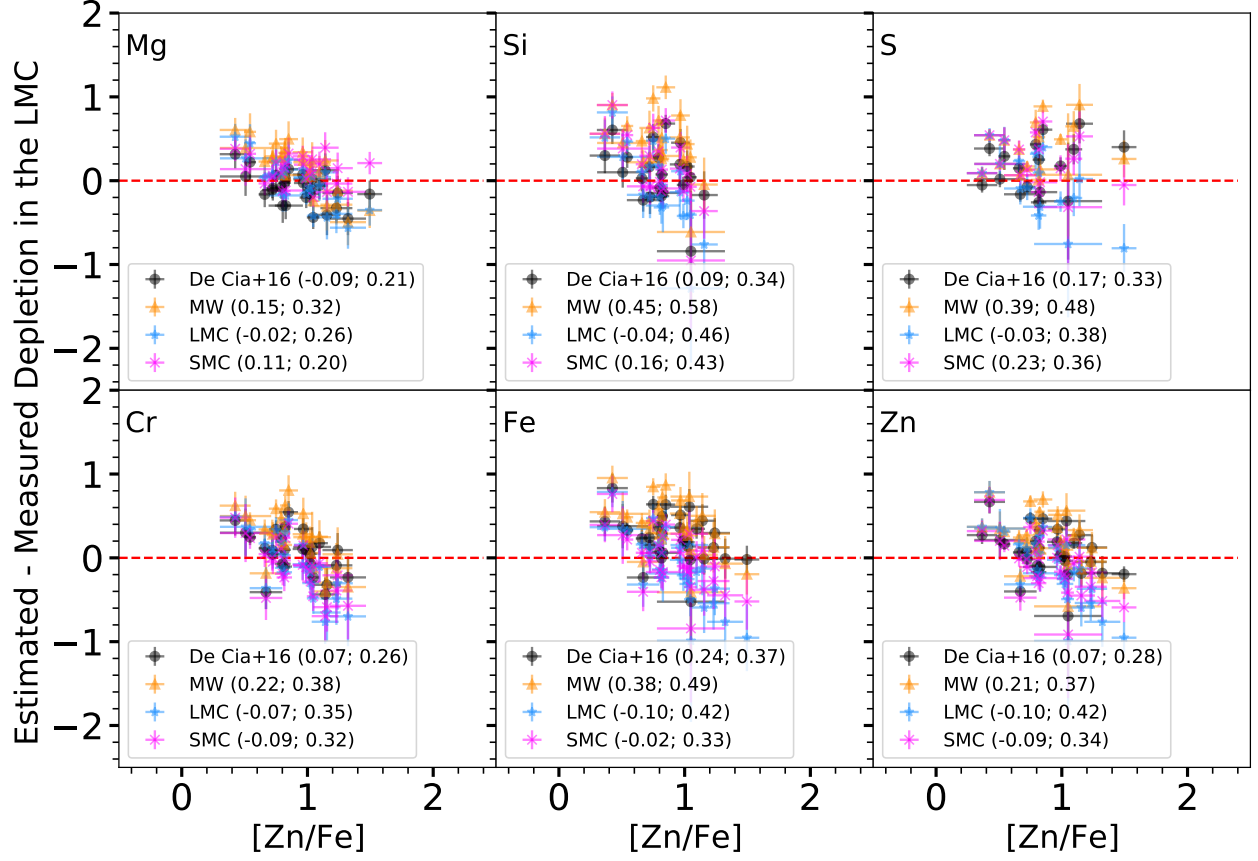


**Figure 19.** Difference in the LMC between measured depletions and depletions estimated using the De Cia et al. (2016) (black), MW (orange), LMC (blue), and SMC (magenta) calibration of the  $[Zn/Fe]-\delta(X)$  relation. The two residuals indicated in parentheses correspond to the mean difference and root mean square difference between the measured and estimated depletions.

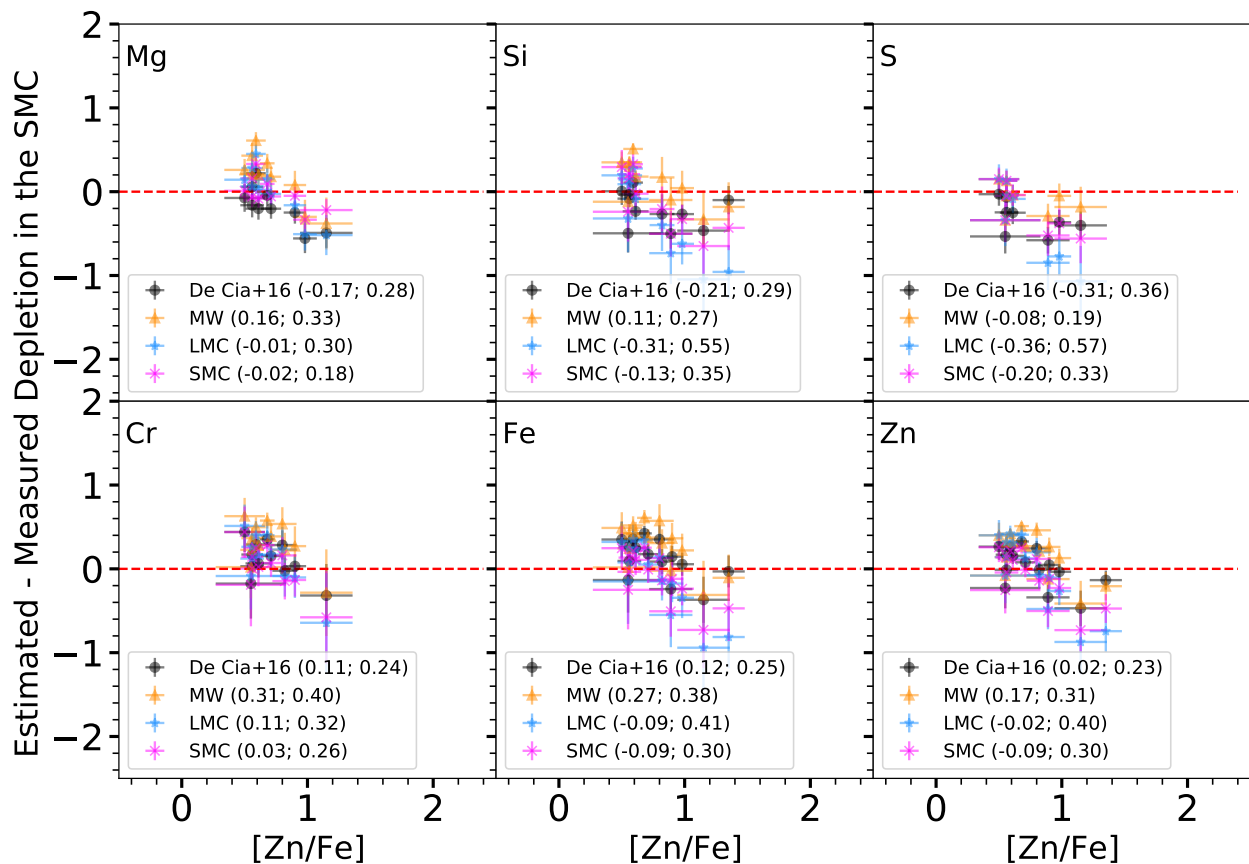


**Figure 20.** Difference in the SMC between measured depletions and depletions estimated using the De Cia et al. (2016) (black), MW (orange), LMC (blue), and SMC (magenta) calibration of the  $[Zn/Fe]-\delta(X)$  relation. The two residuals indicated in parentheses correspond to the mean difference and root mean square difference between the measured and estimated depletions.

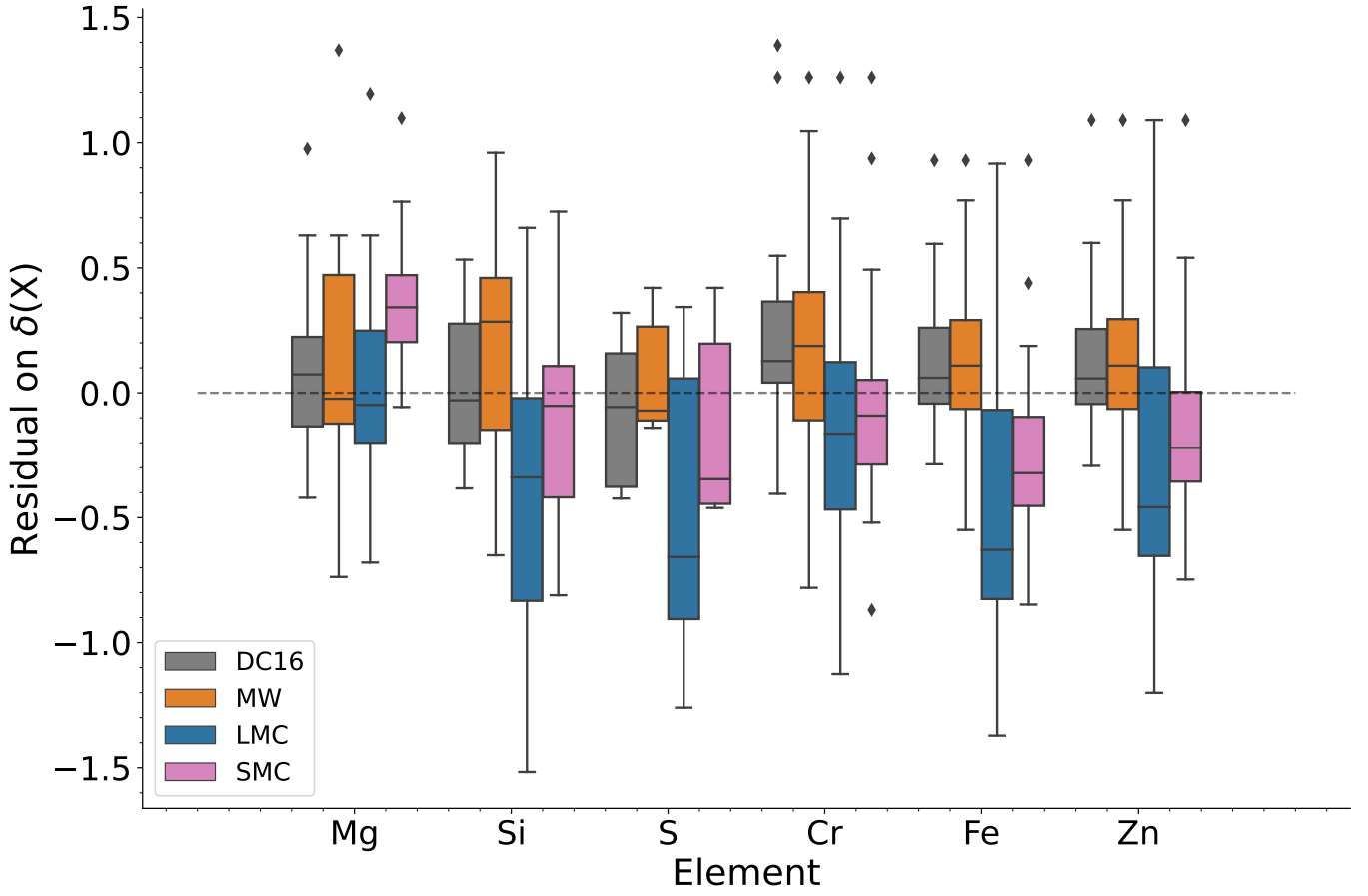


**Figure 21.** Box plot showing the distribution of residuals computed and plotted in Figure 18, for each element and each calibration (DC16, MW, LMC, and SMC) applied to the MW sample of gas-phase abundances. The box shows the quartiles of the dataset while the whiskers extend to show the rest of the distribution.

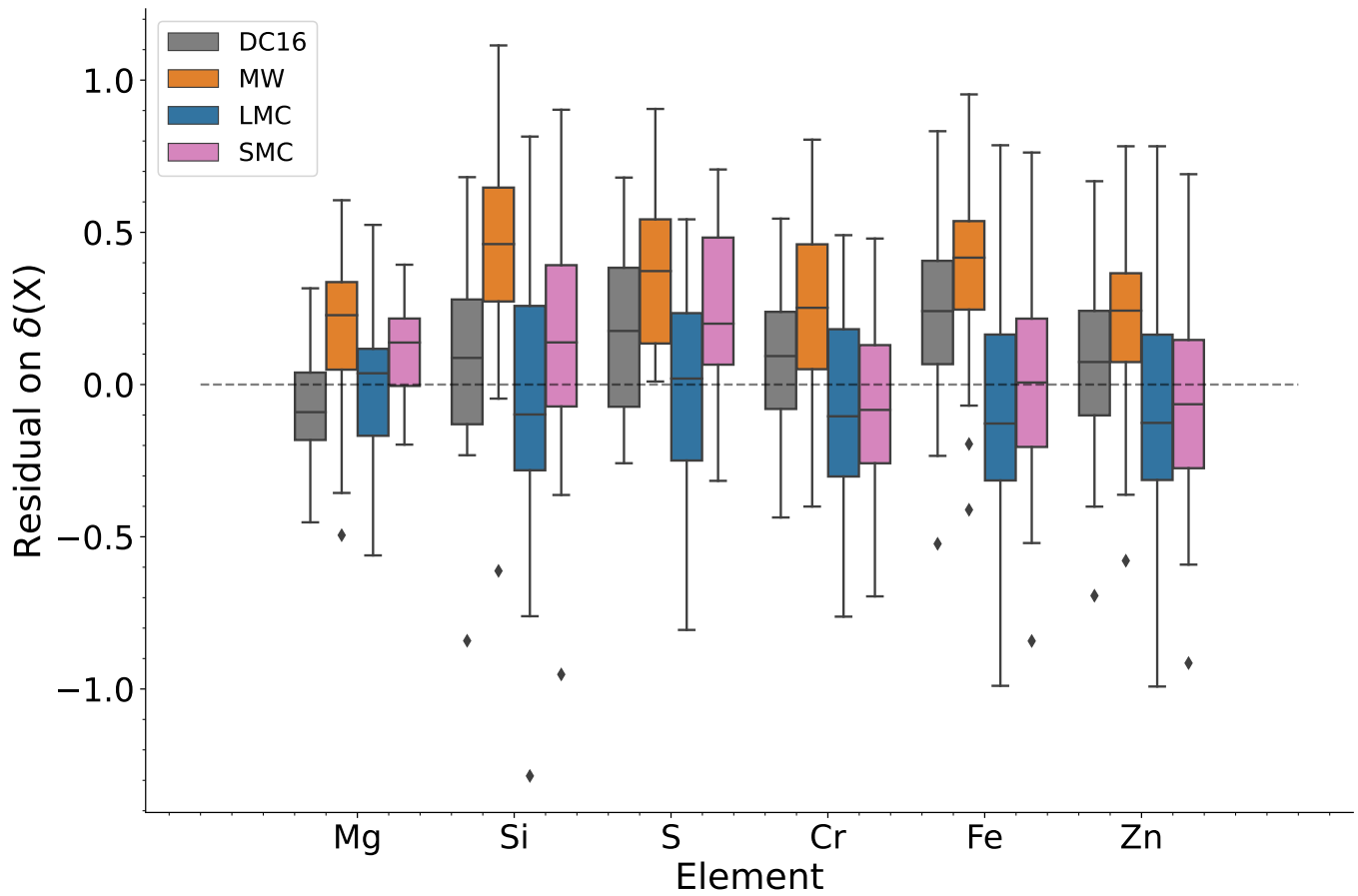


**Figure 22.** Box plot showing the distribution of residuals computed and plotted in Figure 19, for each element and each calibration (DC16, MW, LMC, and SMC) applied to the LMC sample of gas-phase abundances. The box shows the quartiles of the dataset while the whiskers extend to show the rest of the distribution.

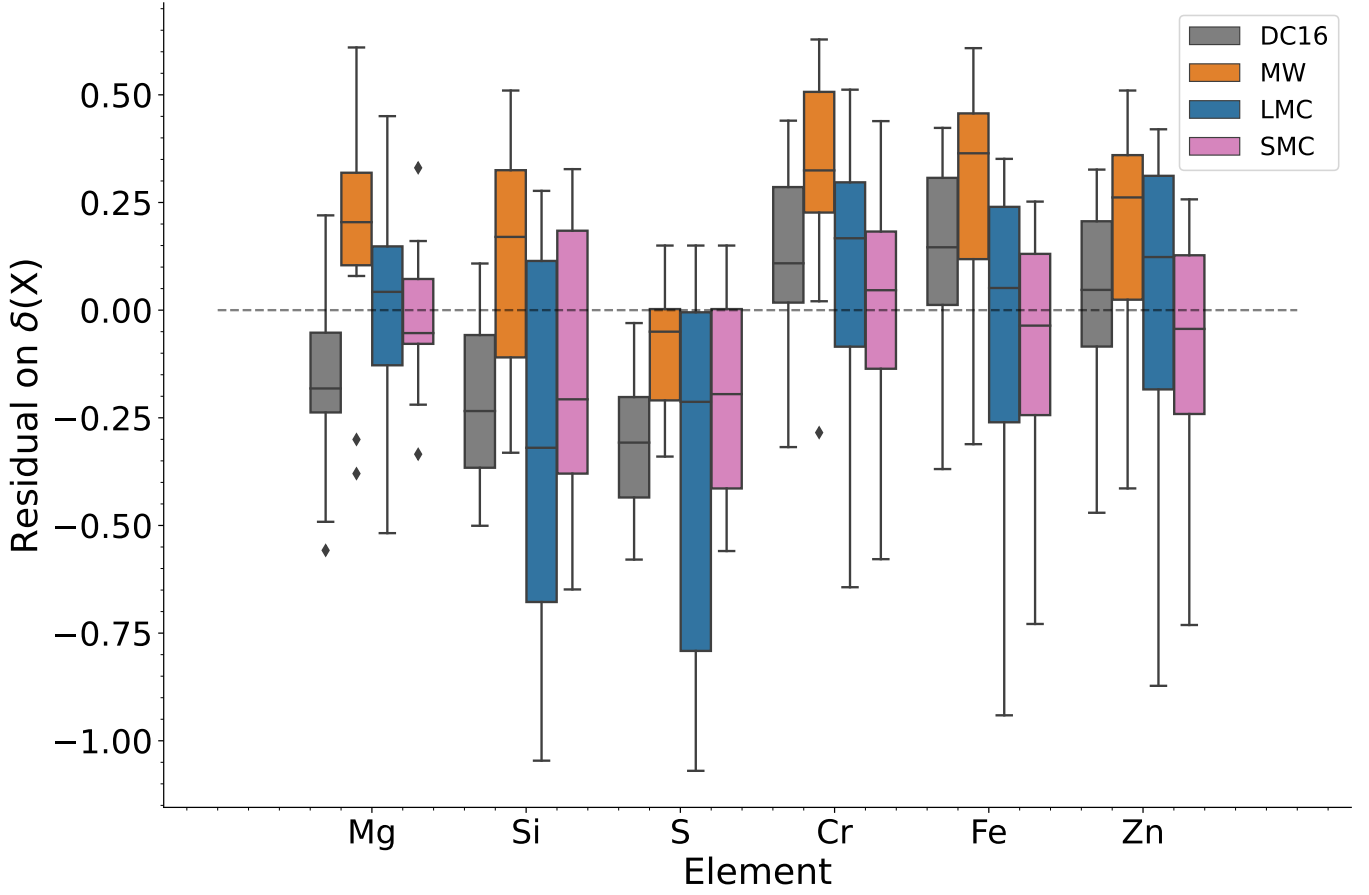


**Figure 23.** Box plot showing the distribution of residuals computed and plotted in Figure 20, for each element and each calibration (DC16, MW, LMC, and SMC) applied to the SMC sample of gas-phase abundances. The box shows the quartiles of the dataset while the whiskers extend to show the rest of the distribution.